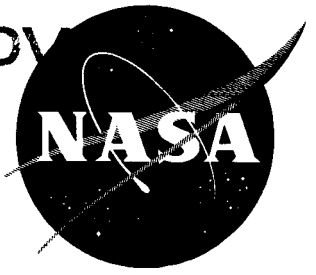


# TECHNICAL NOTE

D-645

## CALCULATION OF WIND COMPENSATION FOR LAUNCHING OF UNGUIDED ROCKETS

By Robert L. James, Jr., and Ronald J. Harris

Langley Research Center
Langley Field, Va.



NATIONAL AERONAUTICS AND SPACE ADMINISTRATION

WASHINGTON April 1961

NATIONAL AERONAUTICS AND SPACE ADMINISTRATION

TECHNICAL NOTE D-645

# CALCULATION OF WIND COMPENSATION FOR LAUNCHING OF UNGUIDED ROCKETS

By Robert L. James, Jr., and Ronald J. Harris

## SUMMARY

A method for calculating wind compensation for unguided missiles is derived which has a greater degree of flexibility than the previously proposed methods. Most of the earlier theories were based on a common set of assumptions which are (1) vehicle motions in pitch and yaw are independent, (2) linear aerodynamic coefficients with respect to flow incidence angle are used, (3) launch angles for wind compensation are the dispersion angles computed by using the weighted wind, and (4) factors used to determine azimuth correction are computed for the standard launch-elevation angle.

Elimination of the first two limitations is the result of using a three-dimensional trajectory simulation with arbitrary wind and nonlinear aerodynamic coefficients with respect to flow incidence angle. The last two limitations were removed by the unique analytical methods used in the present paper.

Utilization of the wind-compensation technique is demonstrated by using the Shotput vehicle as a model. Postflight simulations of four of these missiles with the use of measured winds show that if the winds are known, very good accuracy can be obtained by using the proposed method.

A wind-compensation system for the unguided Scout-SX-1 is presented in the appendix. This system was developed by using the assumptions and methods presented in this paper. The errors obtained are of about the same magnitude as those found for the Shotput system; yet the missile configurations and performance histories are very different.

## INTRODUCTION

The advent of high-altitude-performance missiles has made the consideration of factors causing trajectory deviations or dispersion a necessity. One of the main contributors to the dispersion of an unguided vehicle is wind, and the purpose of this paper is to present a method for minimizing this effect on the trajectory.

During the past decade several theories have been proposed for calculating wind compensation, and results of flights made with the use of these methods have been good in some cases and very poor in others. Most of the previous work was done by using a similar set of assumptions which can cause large errors. These assumptions are:

1. Vehicle motions in pitch and yaw are independent.

2. Linear aerodynamic coefficients with respect to flow incidence angle and small angular perturbations are used.

3. Launch angles for wind compensation are the dispersion angles computed with the use of the weighted wind.

4. Factors used to determine azimuth correction are computed for the standard launch-elevation angle.

The first assumption is poor because the azimuth change is greatly dependent on the elevation angle. The trajectory should be computed in three dimensions so that proper coupling effects between pitch and yaw can be simulated.

Assumption 2 can cause large errors since most vehicles are more sensitive to the wind early in flight when the flow incidence angle can be well into the nonlinear range.

Assumption 3 is a direct misconception of the wind problem and can cause very large errors. The angular dispersion is computed by using the weighted wind, and the compensation angles required are assumed to be equal and opposite to these deviations. It is necessary to perform an iteration to determine the proper launcher angles. This assumption also causes additional errors in pitch since the effect of gravity varies with the launch elevation angle.

The errors introduced by assumption 4 are related to assumption 1. If the wind-compensation procedure calls for a change in the launch elevation, then the yaw-compensation factors should also be changed. This is due to the change in yaw sensitivity associated with the elevation angle.

Probably the most well-known wind-compensation procedure is that described in reference 1. In this paper the rocket is assumed to turn instantaneously into the wind so that the vehicle axis is always tangent to the trajectory. In addition, the wind-weighting factors are assumed to be identical in pitch and yaw.

In reference 2 the theory of reference 1 is improved, as far as the vehicle response is concerned, with the use of more complete missile equations. These equations, however, are still limited to one plane, and also the same weighting factors in pitch and yaw are assumed.

Applications of these theories to different missiles with some slight adjustment are described in references 3 to 6. In some of these applications, different weighting factors in pitch and yaw have been assumed, but the assumptions listed previously are again made.

A much improved wind-compensation scheme was developed for the Little Joe booster and is presented in reference 7. This analysis was based on a six-degree-of-freedom trajectory simulation which is described in reference 8. The vehicle motion is, therefore, very accurate but this wind-compensation method has limitations and disadvantages which are not necessary if the proper procedure is followed. For instance, the analysis is limited to very low altitudes; and although it is true that a large percent of the wind effect occurs at the lower altitude, this is an unnecessary limitation which can be removed without making the procedure more difficult. The system for the Little Joe involves a large number of carpet plots. The method entails an iteration in obtaining the launcher corrections which must be done after the wind is measured. This results in a large amount of computation and graph reading during the last few minutes of the count down.

The wind-compensation procedure which is included in this paper was not developed as an improvement of the technique for the Little Joe. In fact, the two methods are quite different although both were based on the same trajectory simulation.

In the wind-compensation procedure of the present paper, the altitude limitation is not made and the iteration is involved in the development and not during the count down. Also, the scheme only consists of conventional two-dimensional plots which are simple and easy to use. The amount of trajectory simulations and labor necessary to develop the correction graphs is considerably less.

None of the limitations for references 1 and 2 are assumed in this analysis. There are a few simplifying assumptions, causing negligible error in the solution, which are described as they are applied.

## SYMBOLS

In the present paper, distances are measured in U.S. feet (1 U.S. foot = 0.3048006 meter).

$C_{A,O}$ axial-force coefficient at zero flow incidence angle, dimensionless

$C_m$ pitching-moment coefficient, dimensionless

$C_{m_q}$ rate of change of pitching-moment coefficient with pitching velocity, $\frac{\partial C_m}{\partial\left(\frac{qD}{2V'}\right)} = C_{n_r}, \frac{1}{\text{radian}}$

$C_{m_{\dot{\eta}}}$ rate of change of pitching-moment coefficient with rate of change of flow incidence angle, $\frac{\partial C_m}{\partial\left(\frac{\dot{\eta}D}{2V'}\right)}, \frac{1}{\text{radian}}$

$C_N$ normal-force coefficient, dimensionless

$C_n$ yawing-moment coefficient, dimensionless

$C_{n_r}$ rate of change of yawing-moment coefficient with yawing velocity, $\frac{\partial C_n}{\left(\frac{rD}{2V'}\right)}, \frac{1}{\text{radian}}$

$D$ reference length, ft

$I_X$ rolling moment of inertia, slug-ft$^2$

$I_Y$ pitching moment of inertia $\left(I_Y = I_Z\right)$, slug-ft$^2$

$I_Z$ yawing moment of inertia, slug-ft$^2$

$M_Y$ pitching moment, ft-lb

$M_{Y_q}$ rate of change of pitching moment with pitching velocity, $\frac{\partial M_Y}{\partial q} = M_{Z_r}, \frac{\text{ft-lb-sec}}{\text{radian}}$

$M_Z$ yawing moment, ft-lb

$M_{Z_r}$ rate of change of yawing moment with yawing velocity, $\frac{\partial M_Z}{\partial r}$, $\frac{\text{ft-lb-sec}}{\text{radian}}$

$q$ pitching velocity, radians/sec

$r$ yawing velocity, radians/sec

$t_e$ time at which missile is considered insensitive to wind

$V$ missile linear velocity relative to earth, ft/sec

$V'$ total missile linear velocity relative to wind, ft/sec

$V_{w,h}$ horizontal wind velocity relative to earth, ft/sec

$(V_{w,h})_E$ horizontal wind velocity component from the east, ft/sec

$(V_{w,h})_N$ horizontal wind velocity component from the north, ft/sec

$X_E, Y_E, Z_E$ earth-fixed axes, dimensionless

$\dot{x}_E, \dot{y}_E, \dot{z}_E$ components of missile velocity along $X_E$-, $Y_E$-, and $Z_E$-axis, respectively, ft/sec

$x_{cg}$ center-of-gravity distance from nose, ft

$x_{cp}$ center-of-pressure distance from nose, ft

$\gamma_p$ flight-path angle in pitch, deg

$\gamma_{p,o}$ launch elevation angle, deg

$\gamma_y$ flight-path angle in yaw, deg

$\gamma_y'$ flight-path angle in yaw in plane normal to plane of trajectory and tangent to the instantaneous flight path, deg

$\gamma_{y,o}$ launch azimuth compensation for wind, deg

$\eta$ flow incidence angle, radians

$\dot{\eta}$ rate of change of flow incidence angle with time, radians/sec

$\theta_w$ wind direction relative to true north, deg

$\Lambda$ no-wind firing azimuth, deg

$\psi_w$ angle between $V_{w,h}$ and projection of missile center line in $X_E Y_E$-plane, deg

## SHOTPUT CONFIGURATION CHARACTERISTICS

The method for wind compensation presented in the present paper is not limited to any specific missile. However, due to the complex nature of the problem, the procedure as outlined is applied to a particular missile; namely, the Shotput vehicle. The Shotput is a two-stage solid-propellant rocket vehicle used to test the inflation techniques for the 100-foot-diameter balloon satellite. These missiles are fired from NASA Wallops Station.

The Shotput external characteristics are presented in figure 1. The configuration shown is the one which exists at launch and during first-stage burning (in this section, only data pertaining to the vehicle during first-stage burning are presented). The first-stage propulsion system consists of a Pollux rocket motor and two Recruit rockets which are used to increase the acceleration at launch and burnout at about 2 seconds. Aerodynamic stability is obtained by using four $8^\circ$ wedge fins having an area of 15 square feet per panel. The missile is 384.6 inches long and has a maximum diameter of 33 inches.

The aerodynamic parameters for this missile are presented in figure 2. Figure 2(a) shows the aerodynamic coefficients as a function of Mach number for various values of $\eta$. Included are $C_{m_q}$, $C_{m_{\dot{\eta}}}$, $C_{A,0}$, $C_N$, and $x_{cp}$. It was assumed that the vehicle has roll symmetry although the Recruit rocket motors produce an unsymmetric effect. The aerodynamic coefficients are based on a reference area $S$ of 1 sq ft and a reference length $D$ of 1 ft.

Plots of the time varying parameters are presented in figure 2(b) for time from launch to first-stage burnout at 32.5 seconds. Included in this figure are weight, $x_{cg}$, thrust, $I_Y$, $I_X$, and $M_{Y_q}$. Again the assumption was made that the vehicle has roll symmetry.

The nominal performance of the Shotput vehicle is shown in figure 3 as plots of altitude and velocity variations with range. These data were computed in the IBM 704 electronic data processing machine using the aerodynamic parameters presented above and the trajectory program discussed in reference 8. An ICAO standard atmosphere (ref. 9) and a launch angle of 78° were used in these computations.

## ANALYSIS

The wind-compensation procedure derived herein involves four aspects. They are an adequate trajectory simulation, selection of wind profiles, development of wind-compensation graphs, and a wind-weighting procedure.

### Trajectory Simulation

The requirements for a trajectory program needed for a wind-compensation procedure are (1) that the trajectory be three dimensional, (2) that provision be made for arbitrary wind velocity and azimuth and (3) that nonlinear aerodynamics with respect to flow incidence angle be included. The first two requirements are obvious since, in the consideration of side winds, the trajectory is three dimensional and the wind velocity and azimuth are arbitrary. The third requirement is imposed because the introduction of surface winds during launch can create angles of attack larger than 90°, which greatly exceed the linear range of the aerodynamic coefficients.

A trajectory simulation incorporating the above requirements is presented in reference 8. In addition to the above requirements, this simulation assumes a vehicle with six degrees of freedom and aerodynamic symmetry in roll and the missile position in space is computed relative to a flat nonrotating earth. This trajectory simulation was programmed on the IBM 704 electronic data processing machine and is the basis for all trajectory computations made in this paper.

### Selection of Wind Profiles

The winds at some geographical locations have been measured and recorded over periods of time longer than a year. These measurements indicate that the wind velocity generally increases with altitude until a peak is reached at the jet stream and then decreases rather abruptly. Recordings made at Patrick Air Force Base, Cocoa, Florida are presented in reference 10. These annual recordings were used as a basis for selecting profiles to be used in the wind analysis.

The annual profile is shown in figure 4. This curve represents the wind velocities which were measured over a yearly period. The scalar winds indicated on the curve were not exceeded about 96 percent of the time. Also shown in figure 4 are the linear wind profiles which were used in the analysis. The maximum wind profile assumed to be 40 ft/sec is shown as a linear approximation to the annual curve. The other profiles shown in this figure are fractional multiples of the basic curve. It should be noted that a profile is referred to in terms of the surface wind velocity of that profile. There were a total of four wind profiles considered which represented surface winds of 10, 20, 30, and 40 ft/sec.

A missile is insensitive to wind above a certain altitude. For the Shotput vehicle this altitude was determined to be 42,000 feet as is shown in a subsequent section of this paper. Thus, the linear profiles of figure 4 are stopped at this altitude. If the sensitivity range had extended above 42,000 feet, the assumed profiles would be extended also; and their slopes would be changed so that the curve for 40 ft/sec would closely approximate the annual profile.

The assumption that the wind will vary with altitude on the day of firing as one of these profiles is not made in the analysis. The deviation from the profiles of the measured wind is taken into account by weighting the wind which is discussed in a subsequent section.

## Derivation of Wind-Compensation Graphs

In this section the development of a set of wind-compensation graphs is presented. The result is a graph of launch-elevation and launch-azimuth angles as a function of wind azimuth and velocity. Throughout the following analysis, assumptions are made which are difficult to prove directly although they seem correct intuitively. These assumptions are only pointed out as they are passed and are subsequently checked as a group by making sample computer runs with varying wind conditions.

It is convenient to define here some of the terminology used in the analysis. Consider the following diagram:

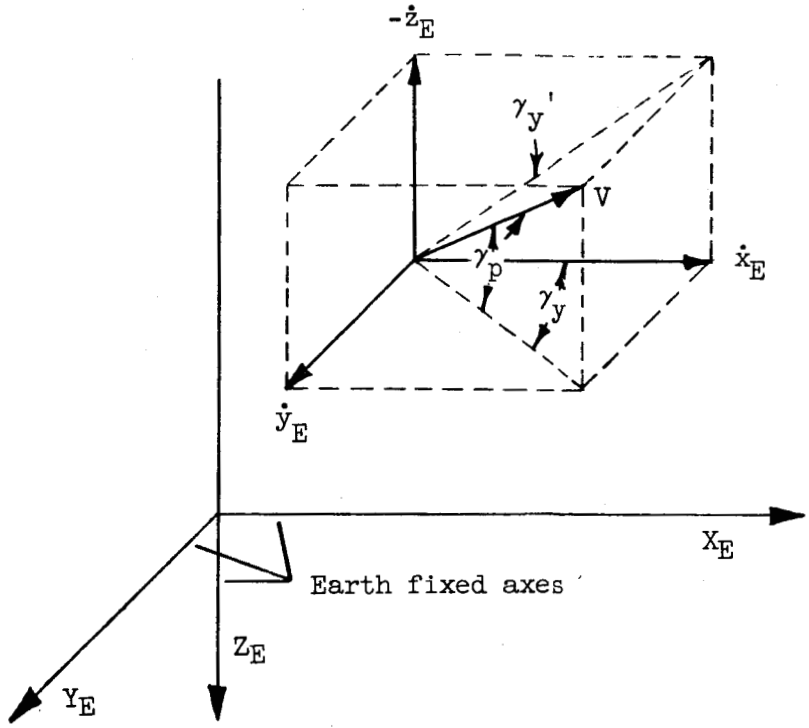


The flight-path angle in pitch is given by

$$\gamma_p = \sin^{-1} \frac{-\dot{z}_E}{V} \tag{1}$$

where V is the missile velocity relative to the ground and can be expressed as

$$V = \sqrt{\dot{x}_E^2 + \dot{y}_E^2 + \dot{z}_E^2} \tag{2}$$

The flight-path angle in yaw can be expressed as

$$\gamma_y' = \sin^{-1} \frac{\dot{y}_E}{V} \tag{3}$$

Note that this angle is in the plane of the missile velocity vector and is not an earth projection. The projection of the yaw flight-path angle in the plane of the earth is given by

$$\gamma_y = \tan^{-1} \frac{\dot{y}_E}{\dot{x}_E} \tag{4}$$

These yaw angles are related to each other through the following equation:

$$\sin \gamma_y' = \sin \gamma_y \cos \gamma_p \tag{5}$$

The time at which the wind is no longer effective is called $t_e$, and for Shotput this value is 25 seconds. This corresponds to an altitude of 42,000 feet which was pointed out above.

The nominal, no-wind launch elevation for Shotput is $78^\circ$, and the nominal values of the preceding flight-path angles at $t_e = 25$ seconds are

$$\gamma_y = 0^\circ$$

$$\gamma_y' = 0^\circ$$

$$\gamma_p = 67.3^\circ$$

Wind conditions cause changes in some or all of these angles depending on the wind direction.

Head and tail winds.- Consider first the effects of head and tail winds. Since the missile is stable and thrusting during the portion of the trajectory being analyzed, it weathercocks. A head wind pitches the missile down and a tail wind pitches it up. Trajectories were computed with various head- and tail-wind profiles and the results of these computations are shown in figure 5 as a plot of the flight-path angle in pitch, $\gamma_p$, at $t_e$ (25 sec) against wind velocity at the surface. The conditions of these trajectory simulations are shown in table I as runs 1 to 9. The launch elevation was held constant at $78^\circ$ for all of these trajectories.

Trajectories were also computed with no wind for various launch elevation angles, and the change in flight-path angle was computed by using the equation

$$\Delta\gamma_p = \gamma_{p,o} - (\gamma_p)_{t_e} \quad . \quad (6)$$

where $\gamma_{p,o}$ is the flight-path angle at launch. In figure 6, $\Delta\gamma_p$ is plotted against launch elevation for the no-wind cases, and also curves are shown for head winds and tail winds. The no-wind trajectory simulations are shown in table I as run 1 and runs 10 to 12. Data for the head winds and tail winds were available for a launch elevation of $78^\circ$ as presented in figure 5 (runs 2 to 9) and for a wind of 40 ft/sec with varying launch elevation in runs 13 to 18. The family of curves shown in this figure was obtained by interpolation between these data points.

It was stated previously that the desired value of $(\gamma_p)_{t_e}$ was $67.3^\circ$. Therefore, for the ideal case, equation (6) can be written,

$$\gamma_{p,o} - \Delta\gamma_p = 67.3^\circ \quad . \quad (7)$$

This expression can be solved graphically with the use of a $45^\circ$ line ($\gamma_{p,o}$ plotted against $\gamma_{p,o}$) which is also plotted in figure 6. A pair of dividers set at $67.3^\circ$ can be moved until the value set is the difference between the $45^\circ$ line and one of the curves. The length corresponding to $67.3^\circ$ is illustrated in figure 6 in the position for determining $\gamma_{p,o}$ for a head wind of 20 ft/sec. It can be seen that the value of $\gamma_{p,o}$ is $82.8^\circ$ for this wind condition. The result of this graphical solution is the curve shown in figure 7. This figure gives the launch elevation needed for wind compensation if the existing wind is a head or tail wind. Hence, if compensation for head and tail winds were the only consideration, figure 7 would suffice.

By making a comparison of figures 5 and 7 it is readily seen that the trial and error process described above is very necessary. A head-wind profile of 40 ft/sec gives a value of $(\gamma_p)_{t_e}$ of $51^\circ$ (fig. 5) which is $16.3^\circ$ lower than the desired value of $67.3^\circ$. Now, if this change is added to the launch-elevation angle of $78^\circ$ it gives $94.3^\circ$ for the corrected launch angle as compared to $87.8^\circ$ which is shown in figure 7. This is an error of $6.5^\circ$ in the launch-elevation angle which, of course, could not be tolerated. Carrying out a similar comparison for a tail wind of 40 ft/sec indicates that an error of $8.5^\circ$ would be made.

Side winds.- The next step in the analysis is the consideration of side-wind components or winds from any direction. The angle $\psi_w$ is

defined as the angle between the launch azimuth and the horizontal component of wind (the horizontal wind component is assumed to be the total wind vector) as shown in the following diagram:

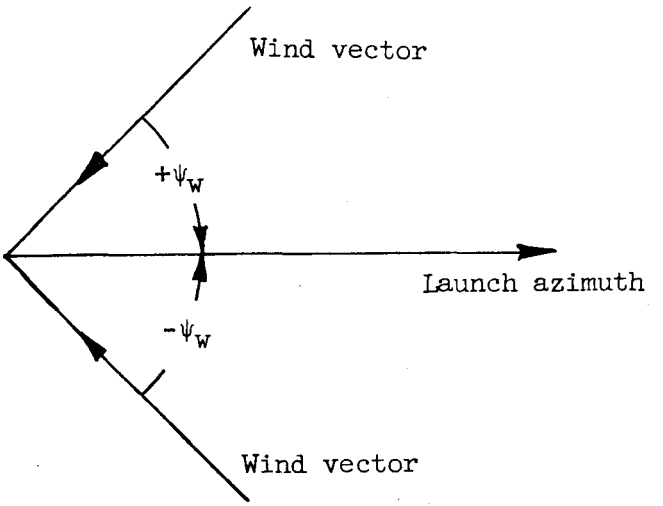


The vectors illustrated in the diagram are all in the horizontal plane.

Trajectory simulations were made for various values of $\psi_w$ and wind profiles assuming a launch-elevation angle of $78^\circ$. The conditions of these computations are shown in table I as runs 1 to 9 and runs 19 to 30. Also shown in the table are values for $\gamma_p$ and $\gamma_y'$ which are listed at $t_e$. These values were computed by using equations (1) and (3) and were plotted against $\psi_w$ for the different wind velocities as in figure 8. The curves were plotted for positive values of $\psi_w$; however, the data can be used for either positive or negative values of $\psi_w$ with the signs of $(\gamma_y')_{t_e}$ being opposite from those of $\psi_w$.

The next figure constructed was made up of data presented in figures 5 and 7. Figure 5 gives $(\gamma_p)_{t_e}$ for various head- and tail-wind velocities, and figure 7 gives the launch elevation needed to compensate for these winds as a function of wind velocity. By making a cross plot of the data in these figures, it is possible to construct a curve of $(\gamma_p)_{t_e}$ plotted against the correct launch elevation. This result is shown in figure 9. Thus, for any value of $(\gamma_p)_{t_e}$ obtained from a

trajectory in which the launch elevation was $78^{\circ}$, it is possible to obtain from this figure the launch elevation which is required to make $(\gamma_p)_{t_e}$ equal to $67.3^{\circ}$ or the nominal, no-wind value. For example, suppose a trajectory were computed by using a launch-elevation angle of $78^{\circ}$ and some head- or tail-wind profile. If the $(\gamma_p)_{t_e}$ under these conditions came out to be $80^{\circ}$, then the launch elevation needed to fly the no-wind trajectory can be read from figure 9 as $71.3^{\circ}$.

It is assumed that the curve of figure 9 is valid for wind conditions other than head and tail winds. In other words, if a value of $(\gamma_p)_{t_e}$ is obtained with a launch angle of $78^{\circ}$ for any wind velocity or direction, the launch elevation necessary to compensate for the error in pitch can be read from the figure. By making this assumption, it is possible to determine the correct launch elevation for each value of $(\gamma_p)_{t_e}$ in figure 8. Values of $(\gamma_p)_{t_e}$ are read in figure 8 and then the correct launch angle is determined from figure 9. The results are shown in figure 10. In this figure is plotted the correct launch elevation as a function of $\psi_w$ for various velocity profiles. This curve gives the wind compensation in the launch elevation for any wind azimuth and various velocity profiles. Note that this figure applies for positive or negative values of $\psi_w$.

The problem remaining is the determination of the azimuth compensation graph. By rearranging equation (5) the following expression is obtained for the yaw angle in the plane of the earth:

$$\gamma_y = \sin^{-1}\left(\frac{\sin \gamma_y'}{\cos \gamma_p}\right) \tag{8}$$

It can readily be seen that as $\gamma_p$ increases, the value of $\gamma_y$ becomes larger than the value of $\gamma_y'$. The reason for this is that $\gamma_y'$ is the yaw angle in the plane of the missile and $\gamma_y$ is the projection of this angle in the earth plane. Hence, as the pitch angle increases, the projection becomes larger for a given value of $\gamma_y'$. For this reason, the dispersion problem becomes very critical when unguided rockets are launched at steep launch angles.

It is assumed that the data for $(\gamma_y')_{t_e}$ in figure 8 can be used for any launch elevation in the neighborhood of $78^\circ$ (this assumption along with others will be proven valid in a subsequent section).

After wind compensation, the pitch angle $\gamma_p$ will be $67.3^\circ$ at 25 seconds. By using the values of $(\gamma_y')_{t_e}$ from figure 8 and $\gamma_p = 67.3^\circ$ in equation (8), it is possible to determine values of $\gamma_y$ for each wind direction and velocity profile. These values were computed and are shown in figure 11.

Consider the following diagram showing the geometry of the wind problem in the horizontal plane:

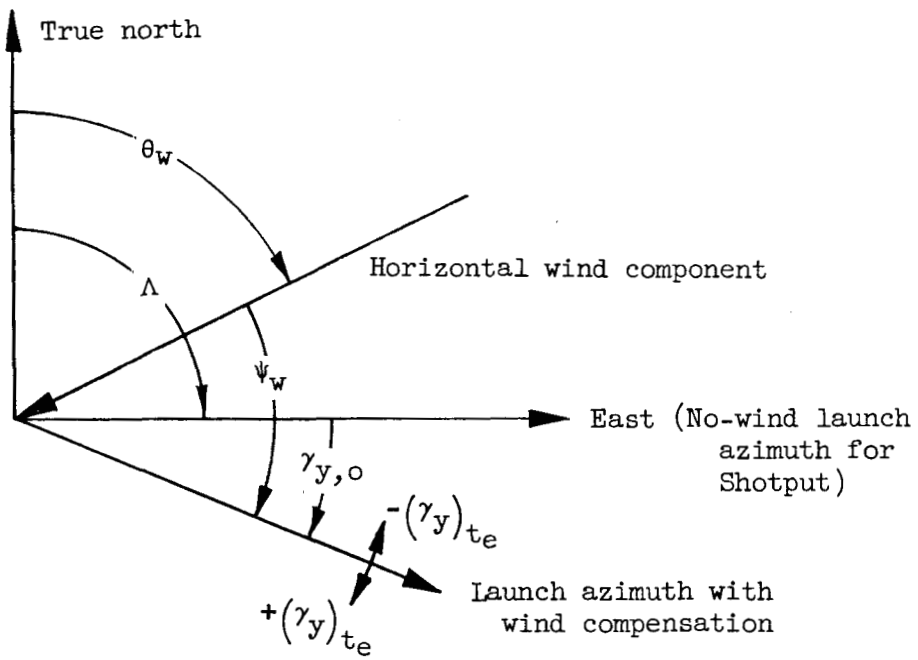


It can be seen in the diagram that

$$\theta_w + \psi_w = \Lambda + \gamma_{y,o} \tag{9}$$

where $\theta_w$ is the wind direction relative to true north, $\gamma_{y,o}$ is the azimuth compensation for wind, and $\Lambda$ is the desired azimuth at $t_e$.

By transposing and substituting $90^\circ$ for $\Lambda$ (since east was the desired direction of fire for Shotput), the following equation is obtained:

$$\psi_w - \gamma_{y,o} = 90^\circ - \theta_w \tag{10}$$

This equation is solved by using a graphical solution similar to that used previously in solving equation (7). The values of $(\gamma_y)_{t_e}$ in figure 11 are measured relative to the launch azimuth of the missile; therefore, $(\gamma_y)_{t_e}$ must be equal in magnitude and opposite in sign to $\gamma_{y,o}$ if the vehicle is on course at $t_e$. (See the preceding diagram.) A $45^\circ$ line is also shown in figure 11 (plot of $\psi_w$ against $\psi_w$) so the values of $\psi_w - \gamma_{y,o}$ or $\psi_w - (-\gamma_y)_{t_e}$ can be obtained for various values of $90^\circ - \theta_w$ which are assumed. The following table includes some sample calculations using this procedure. The arrow shown in figure 11 corresponds to the first calculation in this table.

| Wind profile (assumed), ft/sec | $\theta_w$ (assumed), deg | $90^\circ - \theta_w$ (computed), deg | $(-\gamma_y)_{t_e} = \gamma_{y,o}$ (from fig. 11), deg | $\psi_w$ (from fig. 11), deg | $\gamma_{p,o}$ (from fig. 10), deg |
|---|---|---|---|---|---|
| 40 | 70 | 20 | 38.2 | 58.2 | 84.6 |
| 30 | 140 | -50 | -36.9 | -86.9 | 80.8 |
| 40 | 220 | -130 | -23.8 | -153.8 | 70.7 |
| 30 | 320 | -230 = 130 | 19.3 | 149.3 | 72.8 |

After the value of $\psi_w$ is determined, it is possible to determine the launch-elevation angle from figure 10. Values of launch elevation are also given in the above table.

If this procedure is carried out for each velocity profile and wind-direction angle $\theta_w$ from $0^\circ$ to $360^\circ$, it is possible to construct the final wind-compensation graph as shown in figure 12. This graph gives the launch azimuth and elevation angles needed to compensate for any wind direction and for the various velocity profiles. It should be noted that the desired azimuth is $90^\circ$ and that the curves would be shifted right or left for other values.

These curves only apply to wind-velocity profiles like those assumed previously and wind directions which are invariant with altitude. Therefore, the curves are not very useful alone since wind data at firing time

will generally show direction changes with altitude and the velocity will probably not duplicate the assumed gradient.

In order to alleviate this limitation, a wind-weighting procedure is used which effectively determines the velocity profile and wind direction which most nearly agree with the actual wind conditions. This procedure is discussed in the next section.

## Wind-Weighting Procedure

Previously in this paper it was pointed out that assumed wind profiles were used in the analysis. Before wind-compensation angles can be obtained by using figure 12, it is necessary to determine the linear profile that most nearly approximates the actual wind conditions at launch time. In other words, some weighting procedure must be used which relates actual wind data to one of the assumed profiles.

The ability to compensate for winds depends greatly on the accuracy of the wind data which are used. A discussion of the various wind measuring techniques and their inherent errors is beyond the scope of this report, but it should be emphasized that accurate wind data are necessary before good results can be obtained with a wind-compensation procedure.

A stable missile is most sensitive to winds early in flight when its velocity is low and the altitude is low. The sensitivity decreases rapidly with increasing altitude; hence, it follows that more weight must be given to the low-altitude wind data. A large percentage of the sensitivity occurs in the first 1,000 feet of altitude in most cases.

Obviously, there is some point along the trajectory of a vehicle after which the wind no longer has any noticeable effect on the flight path. The flight time $t_e$ when the missile reaches this point is taken as the end point for the consideration of wind effects; a corresponding altitude determines the cutoff altitude for the wind profiles.

A stable missile tends to yaw, or weathercock, into the wind. The vehicle does not turn completely into the wind but trims at some angle of yaw determined by the respective velocities of the missile and wind. If the missile is thrusting, the thrust vector is also yawed through the same angle and flight-path deviations become evident. If the weathercocked missile is not thrusting, however, the only effect of wind on the flight path is drift and, in most cases, the missile velocity is high and drift can be neglected.

Burnout time, thus, appears to be a suitable endpoint for the wind consideration. It should be noted that the vehicle may become virtually

insensitive to wind at some time before burnout. Nothing is lost, however, if the chosen endpoint is beyond the sensitive range. Each missile must be treated individually to determine the sensitive region of the trajectory to be considered. Configurations vary so much that there is no rule which can be used in all cases.

There are several schemes for determining sensitivity. The method used here consists of programming a sharp-edged horizontal gust to hit the vehicle at various altitudes along its nominal no-wind trajectory. A constant side wind of 50 ft/sec, which was allowed to remain effective until burnout, was used for all cases considered. In other words, the vehicle is flying the nominal trajectory until the gust altitude is reached and then remains under the effect of the wind until burnout. The altitudes chosen for the wind to become effective were arbitrary, but most were at the lower altitudes where the sensitivity is greater.

The wind causes the missile to yaw through an angle $\gamma_y$ which is evident at $t_e$. By knowing the value of $\gamma_y$ at $t_e$ and by assuming that the pitch angle at this point will be the nominal value after wind compensation, it is possible to use equation (8) to determine the values of $\left(\gamma_y'\right)_{t_e}$.

A comparison of the resulting $\left(\gamma_y'\right)_{t_e}$ for different altitudes is a measure of wind sensitivity. A typical plot showing the change of $\left(\gamma_y'\right)_{t_e}$ with gust altitude is given for the Shotput in figure 13(a). Note that the altitudes are the altitudes at which the vehicle enters the gust.

From the figure, it is seen that there is no noticeable change in $\left(\gamma_y'\right)_{t_e}$ past an altitude of 42,000 feet. This is the end of the sensitive range and the wind profiles for Shotput were cut at this point. The corresponding time of flight was 25 seconds which determined $t_e$. The data of figure 13(a) can be put in a more useful form by dividing each value of $\left(\gamma_y'\right)_{t_e}$ by the maximum value occurring, as shown in figure 13(b). The maximum value will usually occur at zero altitude, but this is not a necessity. This curve is a representation of relative sensitivity since it is a comparison of $\left(\gamma_y'\right)_{t_e}$ values as a function of altitude. A change in the ratio $\left(\gamma_y'\right)_{t_e} \Big/ \left(\gamma_y'\right)_{t_{e,max}}$ of 0.01 represents a 1-percent change in sensitivity, and the corresponding altitude bracket is the layer over which the change occurs.

The altitude for each 0.05 change was read and listed in table II. These altitudes define the boundaries of wind layers which have a weight factor of 0.05 assigned to them. Thus, a total of 20 layers was obtained but more or less may be used depending on the vehicle characteristics and the shape of the sensitivity curve. Note that 55 percent of sensitivity occurs in the first 1,000 feet.

The boundaries defining the wind layers were drawn on a plot of the wind profiles as illustrated in figure 14. For any reasonable altitude scale, the small layers below 1,000 feet would be indistinct; therefore, a logarithmic scale was used which tends to make the layers equally important. A disadvantage in using the logarithmic scale is the impossibility of having an exact zero altitude, but this usually creates no problem since the vehicle center of gravity is not at zero altitude at take-off. (The Shotput center of gravity was about 25 feet off the ground while still on the launcher.)

As an example of the wind-weighting procedure, consider the wind data plotted in figure 14. These data were measured before the firing of a Shotput vehicle on October 28, 1959 at NASA Wallops Station using aerovanes and radar-tracked chaff balloons. Table II includes the wind velocity and direction readings for each layer. For example, in layer 20 the wind velocity read was 30 ft/sec which was interpolated from the assumed constant gradient profiles. The wind azimuth is read directly since no profiles exist for the wind azimuth.

After the velocity and azimuth values are tabulated for each layer, the east and north components are determined by using the following expressions:

$$\left(V_{w,h}\right)_E = V_{w,h} \sin \theta_w \tag{11}$$

$$\left(V_{w,h}\right)_N = V_{w,h} \cos \theta_w \tag{12}$$

The components are added algebraically and the weighted wind velocity and azimuth are obtained from these summations as shown in table II. Note that the weighted north and east components are determined by dividing $\sum \left(V_{w,h}\right)_N$ and $\sum \left(V_{w,h}\right)_E$ by 20. The value 20 must be used since each layer has a weight of 0.05 as explained previously. The weighted wind velocity and direction for this particular wind was computed to be 16.4 ft/sec and 305°, respectively. Hence, the actual wind is represented by a constant gradient with a surface velocity of 16.4 ft/sec and a direction of 305°.

Using these values in figure 12 gives 74.7° for the launch elevation and 99° for the launch azimuth. A discussion of the results with the use of these angles is presented in the next section.

## DISCUSSION

### Check of Analysis and Assumptions

The previously described wind analysis was checked by using two different schemes which will be discussed in this section. In the first of these, trajectories were computed by using the assumed profiles while holding the wind direction constant in each simulation and by using the derived launch corrections discussed previously and presented in figure 12. By this procedure it was possible to check the basic assumptions of the wind analysis up to the point of the wind-weighting procedure. The second scheme consisted of computing trajectories with wind data having varying velocity and direction, part of which were measured at NASA Wallops Station on the days of Shotput firings and the remainder of which were arbitrarily selected. This procedure checks the basic assumptions again but, in addition, it checks the wind-weighting procedure.

The results for the first scheme of checking are shown in figure 15(a). Various wind profiles and wind directions were considered which are listed in the figure. Pitch and yaw compensation angles were read from figure 12 for each of these conditions and were used in the trajectory analysis. It can be seen from the figure that the compensation values are in excellent agreement with the total change produced by the wind in each case. It was concluded from this study that the assumptions made in developing the wind-compensation graphs are valid.

The results for varying wind velocity and direction are shown in figure 15(b). Actual wind data measured on the day of firing of four Shotput vehicles were used in this study in addition to one arbitrarily selected wind profile. Winds measured on October 28, 1959, are presented in figure 14, and the remaining wind data are presented in figure 16. These winds were weighted using the procedure described under the previous section of this report and the compensation angles were read from figure 12 using the weighted values. These weighted values are also listed in figure 15(b) with the date the wind was measured. Here again, the compensation values agree very well with the total change produced by the wind. The average error in pitch was 0.3° and the average error in yaw was 1.3°. It was concluded from these results that the weighting procedure is sufficiently accurate.

An error analysis similar to the one discussed previously was carried out for the wind-compensation system for the unguided Scout-SX-1

missile. This system was developed by using the assumptions and methods described in this paper and is presented in the appendix. The errors obtained were of about the same magnitude as those found for the Shotput system yet the missile configurations and performance histories are very different.

## Significance of Limitations Imposed on Previous Wind-Compensation Methods

Several other wind-compensation methods were described in the Introduction of this paper with the limitations imposed on them. In the following paragraphs, an attempt will be made to show the effects of these limitations for the type of vehicle and launch conditions considered herein. The assumptions made in references 1 and 2 were given as:

1. Vehicle motions in pitch and yaw are independent.

2. Linear aerodynamic coefficients with respect to the flow incidence angle and small angular perturbations are used.

3. Launch angles for wind compensation are the dispersion angles computed using the weighted wind.

4. Factors used to determine azimuth correction are computed for the standard launch-elevation angle.

The error caused by the first assumption can readily be seen in the wind-compensation graph of figure 12. A pure side-wind profile ($\theta_w = 0^\circ$, $180^\circ$, or $360^\circ$) with a velocity of 40 ft/sec requires a $\gamma_{p,o}$ for wind compensation of $74.5^\circ$ which is $3.5^\circ$ below the nominal launch angle of $78^\circ$. In the previous methods, no pitch correction is made for pure side winds so this would be a $3.5^\circ$ error in elevation under these conditions.

The second assumption is poor because the flow incidence angle $\eta$ is very large during the early portion of flight. If the Shotput vehicle were subjected to a 40 ft/sec wind at launch, it would travel about 65 feet to an altitude of 90 feet before $\eta$ decreased to a value of $10^\circ$. As can be seen in figure 14, there are almost four wind layers in this altitude region which comprise 20 percent of the total wind effect. Since this is a large portion of the total effect, it is concluded that nonlinear aerodynamic coefficients should be used.

The effect of the third assumption can be seen by referring to figure 11. Suppose there were a pure side-wind profile of 40 ft/sec $(\psi_w = 90^\circ)$ acting on the missile. It can be seen in the figure that the vehicle would yaw 51° under these conditions. Now, if the full 51° were used as the launch-azimuth correction, the new value of $\psi_w$ would be 90° + 51° or 141°. The missile would then yaw only 33° and the azimuth error would be 18° which is very large. The same argument can be applied to the pitch case as was shown previously in the section entitled "Derivation of Wind-Compensation Graphs."

Errors introduced by assumption 4 can be shown by considering equation (8) which was stated as

$$\gamma_y = \sin^{-1}\left(\frac{\sin \gamma_y'}{\cos \gamma_p}\right)$$

Now, let $\gamma_y'$ be a reasonable value of 5° and let $\gamma_p$ be 70° and 80°. Then, $\gamma_y$ corresponding to these values would be 14.8° and 30.2°, respectively. Thus, a difference by factor of approximately 2 is obtained for the two launch angles. Obviously, using the same wind correction for each launch angle can produce intolerable errors.

The main limitation imposed on the wind-compensation method of reference 7 for the Little Joe is the maximum altitude. The author points out the errors that could be obtained with the Little Joe vehicle for various wind conditions under this assumption. For the Shotput, it is interesting to note in figure 14 that 60 percent of the wind weighting remains at an altitude above 455 feet which is about the altitude that the Little Joe analysis was discontinued. It is concluded that the limitation of reference 7 can not generally be made without causing error.

## CONCLUDING REMARKS

A method for calculating wind compensation for unguided missiles has been derived which has a greater degree of flexibility than previously proposed methods. Most of the earlier theories were based on a common set of assumptions which are: (1) vehicle motions in pitch and yaw are independent, (2) linear aerodynamic coefficients with respect to flow incidence angle and small perturbations are used, (3) launch angles for wind compensation are the dispersion angles computed using the weighted wind, (4) factors used to determine azimuth correction are computed for the standard launch-elevation angle.

Elimination of the first two limitations resulted from using a three-dimensional trajectory simulation with arbitrary wind and non-linear aerodynamic coefficients with respect to flow incidence angle. The last two limitations are removed by the unique analytical methods which are presented.

Use of the wind-compensation technique was demonstrated by using the Shotput vehicle as a model. Postflight simulations of four of these missiles with the use of measured winds showed that, if the winds were known, very good accuracy could be obtained using the proposed method.

A wind-compensation system for the unguided Scout-SX-1 is presented in the appendix. This system was developed by using the assumptions and methods presented in this paper. The errors obtained are of about the same magnitude as those found for the Shotput system; yet the missile configurations and performance histories are very different.

A more detailed preflight trajectory analysis is required for the use of this technique than is necessary with the use of conventional methods. However, in order to obtain the desired missile performance with minimum wind dispersion, a wind-compensation scheme having the capabilities of the one presented must be used.

Langley Research Center,
National Aeronautics and Space Administration,
Langley Field, Va., October 17, 1960.

# APPENDIX

## WIND COMPENSATION FOR THE SCOUT-SX-1

The Scout-SX-1 vehicle was the first test of the Scout series. This missile was fired without guidance; thus it was necessary to use a wind-compensation procedure. The procedure described in this paper was selected and the compensation graphs and results are presented.

The Scout-SX-1 external characteristics are presented in figure 17. This is the configuration that exists at launch and during first-stage burning. The first-stage propulsion system is an Algol solid-propellant rocket motor. The missile is 760.1 inches long and has a maximum diameter of 40 inches. Four $8^{\circ}$ wedge fins having an area of 4.5 square feet per panel provide aerodynamic stability.

The aerodynamic parameters for this missile are presented in figure 18. Figure 18(a) shows the aerodynamic coefficients as functions of Mach number, and the time varying parameters are shown in figure 18(b). These are the same terms as previously presented for the Shotput vehicle except that $C_{m_{\dot{\eta}}}$ was small and assumed to be zero for this missile. Roll symmetry was again assumed and the reference area S and length D are 1 square foot and 1 foot, respectively.

The nominal performance of the Scout-SX-1 vehicle is shown in figure 19 as plots of altitude and velocity variations with range. The launch angle was $81^{\circ}$ and the ICAO standard atmosphere (ref. 9) was assumed. It can be seen by comparing figures 3 and 19 that the launch acceleration is much smaller for Scout-SX-1 than for Shotput. The Shotput launch acceleration was 11.9g; whereas for Scout-SX-1 this value was 2.7g. The combination of lower acceleration at take-off and the steeper launch elevation ($81^{\circ}$ for Scout, $78^{\circ}$ for Shotput) are factors which make the Scout vehicle more sensitive to wind than the Shotput.

A sensitivity curve was computed using the method previously described. The plot of $\left(\gamma_y'\right)_{t_e} \Big/ \left(\gamma_y'\right)_{t_{e,max}}$ is presented in figure 20. This curve is very similar to the one presented for Shotput in figure 13, which is reasonable since this curve only shows the relative sensitivity for different altitudes.

The wind-compensation graph for the Scout-SX-1 is shown as figure 21. When compared with the Shotput curve of figure 12, it can be seen that the pitch corrections are very similar for the same wind velocity and direction. (Note that Scout curve has a maximum wind velocity profile of

30 ft/sec.) The azimuth corrections are quite different, however. The maximum correction for Scout with a 30 ft/sec profile is about $48^{\circ}$ but this value for Shotput is $38^{\circ}$. Since the sensitivity in pitch is almost the same for the two vehicles, the lower acceleration of the Scout must be somewhat compensated for by its smaller ratio of aerodynamic moment to pitch inertia. The increased yaw sensitivity must then be mostly due to the higher launch angle of the Scout.

Wind data measured on the day of firing for the Scout-SX-1 are presented in figure 16. These data were weighted which gave 26.9 ft/sec and $310^{\circ}$ for the weighted wind velocity and direction, respectively. The compensation angles were obtained from figure 21 using these values.

For the postflight simulation, it was found that the $\gamma_p$ change obtained in simulation was $4.6^{\circ}$ as compared with the $4.8^{\circ}$ actually used and that the $\gamma_y$ change obtained in simulation was $17.2^{\circ}$ compared with the $17.8^{\circ}$ actually used. The data show a $0.2^{\circ}$ error in pitch and a $0.6^{\circ}$ error in yaw as compared with the average errors obtained for Shotput of $0.3^{\circ}$ and $1.3^{\circ}$.

## REFERENCES


1. Lewis, J. V.: The Effect of Wind and Rotation of the Earth on Unguided Rockets. Rep. No. 685, Ballistic Res. Labs., Aberdeen Proving Ground, Mar. 1949.

2. Daw, Harold A.: A Wind Weighting Theory for Sounding Rockets Derivable From the Rocket Equations of Motion. Contract N9ONR-9530 1, Phys. Sci. Lab., New Mexico College of Agric. and Mechanic Arts, Nov. 5, 1958.

3. Rachele, Henry (revised by William H. Hatch): The Effect of Wind and Tower Tilt on Unguided Rockets. Rev. Prog. Rep. Nr 6, Missile Geophys. Div., U.S. Army White Sands Signal Agency, Feb. 1958.

4. Webb, Willis L., Jenkins, Kenneth R., and Clark, George Q.: Flight Testing of the Arcas. Tech. Memo. 623, Missile Geophys. Div., U.S. Army White Sands Signal Agency, May 1959.

5. Zaroodny, Serge J., Mylin, Donald C., and McIntosh, Fred H.: Spin of an Honest-John-Type Rocket - Experimental Data and Their Implications for the Design. Rep. No. 1090, Ballistic Res. Labs., Aberdeen Proving Ground, Dec. 1959.

6. Anon.: Dispersion Analysis Journeyman Sounding Rocket. Rep. No. 8411-1, Aerolab Dev. Co., Inc. (Pasadena), Sept. 16, 1959.

7. Rose, James T., and Rose, Rodney G.: A Rapid Method of Estimating Launcher Setting to Correct for the Effects of Wind on the Trajectory of an Unguided Fin-Stabilized Rocket Vehicle. NASA TM X-492, 1961.

8. James, Robert L., Jr. (With Appendix B by Norman L. Crabill): A Three-Dimensional Trajectory Simulation Using Six Degrees of Freedom With Arbitrary Wind. NASA TN D-641, 1961.

9. Anon.: Standard Atmosphere - Tables and Data for Altitudes to 65,800 Feet. NACA Rep. 1235, 1955. (Supersedes NACA TN 3182.)

10. Anon.: Wind Distributions as a Function of Altitude for Patrick Air Force Base, Cocoa, Florida. Rep. No. DA-TR-12-58, Dev. Operations Div., Army Ballistic Missile Agency (Redstone Arsenal, Ala.), Aug. 5, 1958.

TABLE I

COMPUTER RUNS USED IN SHOTPUT WIND ANALYSIS

| Run number | Launch elevation, deg | $\psi_w$, deg | Wind velocity profile, ft/sec | $(\gamma_p)_{t_e}$, deg | $(\gamma_y')_{t_e}$, deg |
|---|---|---|---|---|---|
| 1 | 78 | 0 | 0 | 67.3 | 0 |
| 2 | 78 | 0 | 10 | 63.2 | 0 |
| 3 | 78 | 0 | 20 | 59.0 | 0 |
| 4 | 78 | 0 | 30 | 54.8 | 0 |
| 5 | 78 | 0 | 40 | 50.9 | 0 |
| 6 | 78 | 180 | 10 | 71.8 | 0 |
| 7 | 78 | 180 | 20 | 76.4 | 0 |
| 8 | 78 | 180 | 30 | 82.2 | 0 |
| 9 | 78 | 180 | 40 | 85.4 | 0 |
| 10 | 58 | 0 | 0 | 33.4 | 0 |
| 11 | 68 | 0 | 0 | 50.1 | 0 |
| 12 | 88 | 0 | 0 | 86.2 | 0 |
| 13 | 58 | 0 | 40 | 22.5 | 0 |
| 14 | 68 | 0 | 40 | 36.0 | 0 |
| 15 | 88 | 0 | 40 | 68.0 | 0 |
| 16 | 58 | 180 | 40 | 47.0 | 0 |
| 17 | 68 | 180 | 40 | 66.5 | 0 |
| 18 | 88 | 180 | 40 | 105.2 | 0 |
| 19 | 78 | 45 | 10 | 63.7 | -3.1 |
| 20 | 78 | 45 | 20 | 60.2 | -6.0 |
| 21 | 78 | 45 | 30 | 56.7 | -8.8 |
| 22 | 78 | 45 | 40 | 54.3 | -11.4 |
| 23 | 78 | 90 | 10 | 66.2 | -5.0 |
| 24 | 78 | 90 | 20 | 64.7 | -8.6 |
| 25 | 78 | 90 | 30 | 63.7 | -13.4 |
| 26 | 78 | 90 | 40 | 62.7 | -17.6 |
| 27 | 78 | 135 | 10 | 69.5 | -3.3 |
| 28 | 78 | 135 | 20 | 72.1 | -6.5 |
| 29 | 78 | 135 | 30 | 74.2 | -10.0 |
| 30 | 78 | 135 | 40 | 75.7 | -13.4 |

TABLE II

WIND-WEIGHTING PROCEDURE

| Layer | Altitude, ft | $V_{w,h}$, ft/sec | $\theta_w$, deg | Sin $\theta_w$ | Cos $\theta_w$ | $(V_{w,h})_E = V_{w,h} \sin \theta_w$ | $(V_{w,h})_N = V_{w,h} \cos \theta_w$ |
|---|---|---|---|---|---|---|---|
| 1 | 25 to 35 | 13 | 309 | -0.7772 | 0.6293 | -10.10 | 8.18 |
| 2 | 35 to 45 | 14 | 309 | -.7772 | .6293 | -10.88 | 8.81 |
| 3 | 45 to 65 | 14 | 308 | -.7880 | .6157 | -11.03 | 8.62 |
| 4 | 65 to 115 | 15 | 308 | -.7880 | .6157 | -11.82 | 9.24 |
| 5 | 115 to 175 | 15 | 308 | -.7880 | .6157 | -11.82 | 9.24 |
| 6 | 175 to 245 | 16 | 308 | -.7880 | .6157 | -12.61 | 9.85 |
| 7 | 245 to 345 | 16 | 307 | -.7986 | .6018 | -12.78 | 9.63 |
| 8 | 345 to 455 | 16 | 307 | -.7986 | .6018 | -12.78 | 9.63 |
| 9 | 455 to 615 | 16 | 307 | -.7986 | .6018 | -12.78 | 9.63 |
| 10 | 615 to 825 | 16 | 307 | -.7986 | .6018 | -12.78 | 9.63 |
| 11 | 825 to 1,075 | 16 | 307 | -.7986 | .6018 | -12.78 | 9.63 |
| 12 | 1,075 to 1,415 | 16 | 308 | -.7880 | .6157 | -12.61 | 9.85 |
| 13 | 1,415 to 1,900 | 16 | 310 | -.7660 | .6428 | -12.26 | 10.28 |
| 14 | 1,900 to 2,700 | 16 | 315 | -.7071 | .7071 | -11.31 | 11.31 |
| 15 | 2,700 to 4,050 | 16 | 321 | -.6293 | .7772 | -10.07 | 12.44 |
| 16 | 4,050 to 6,500 | 18 | 318 | -.6691 | .7431 | -12.04 | 13.38 |
| 17 | 6,500 to 10,500 | 17 | 310 | -.7660 | .6428 | -13.02 | 10.93 |
| 18 | 10,500 to 15,000 | 17 | 303 | -.8387 | .5446 | -14.26 | 9.26 |
| 19 | 15,000 to 22,000 | 22 | 290 | -.9397 | .3420 | -20.67 | 7.52 |
| 20 | 22,000 to 42,000 | 30 | 273 | -.9986 | .0523 | -29.96 | 1.57 |
| | | | | | | $\Sigma$ = -268.36 | 188.63 |

Computation of weighted values -

$$V_{w,h} = \sqrt{\left[\frac{\sum (V_{w,h})_E}{20}\right]^2 + \left[\frac{\sum (V_{w,h})_N}{20}\right]^2} = 16.4 \text{ ft/sec}$$

$$\theta_w = \tan^{-1}\left[\frac{\sum (V_{w,h})_E}{\sum (V_{w,h})_N}\right] = 305^\circ$$

From figure 12 -

$\gamma_{p,o} = 74.7^\circ$

$\gamma_{y,o} = 9.0^\circ$

Launch azimuth = $99.0^\circ$

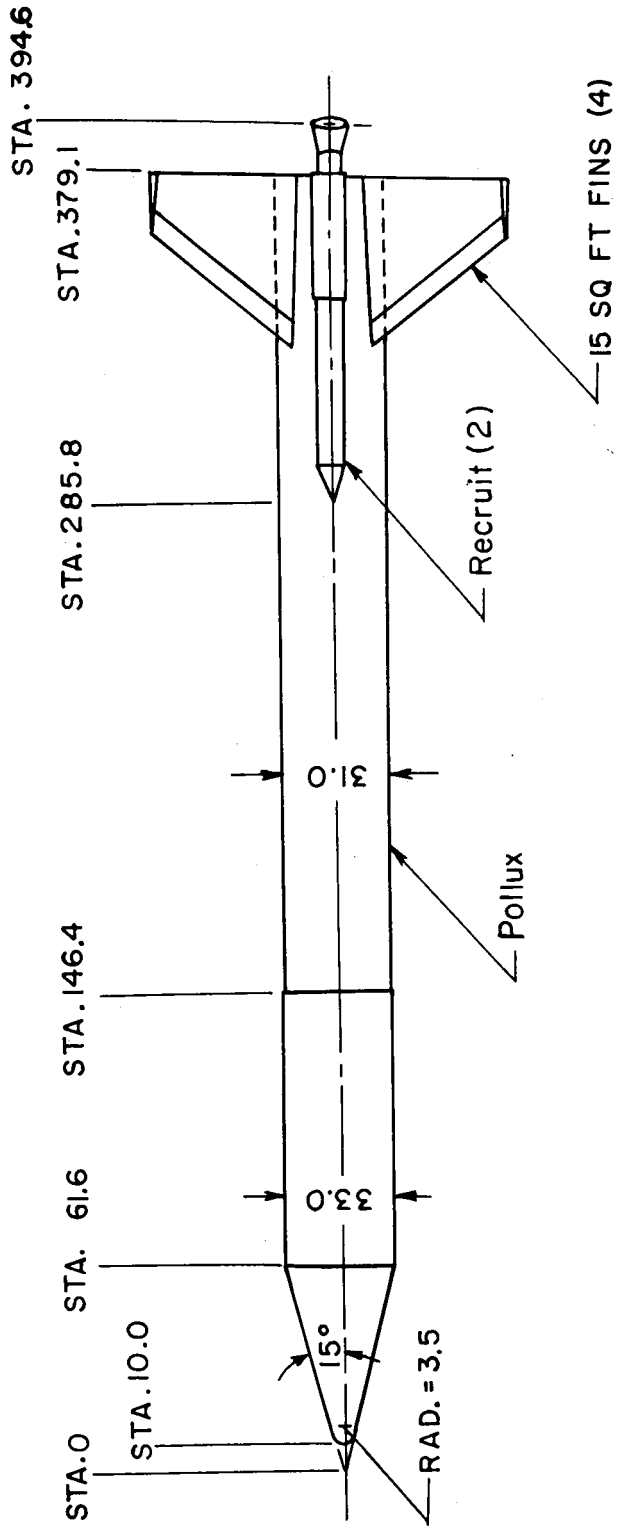


Figure 1.- General configuration of Shotput vehicle.

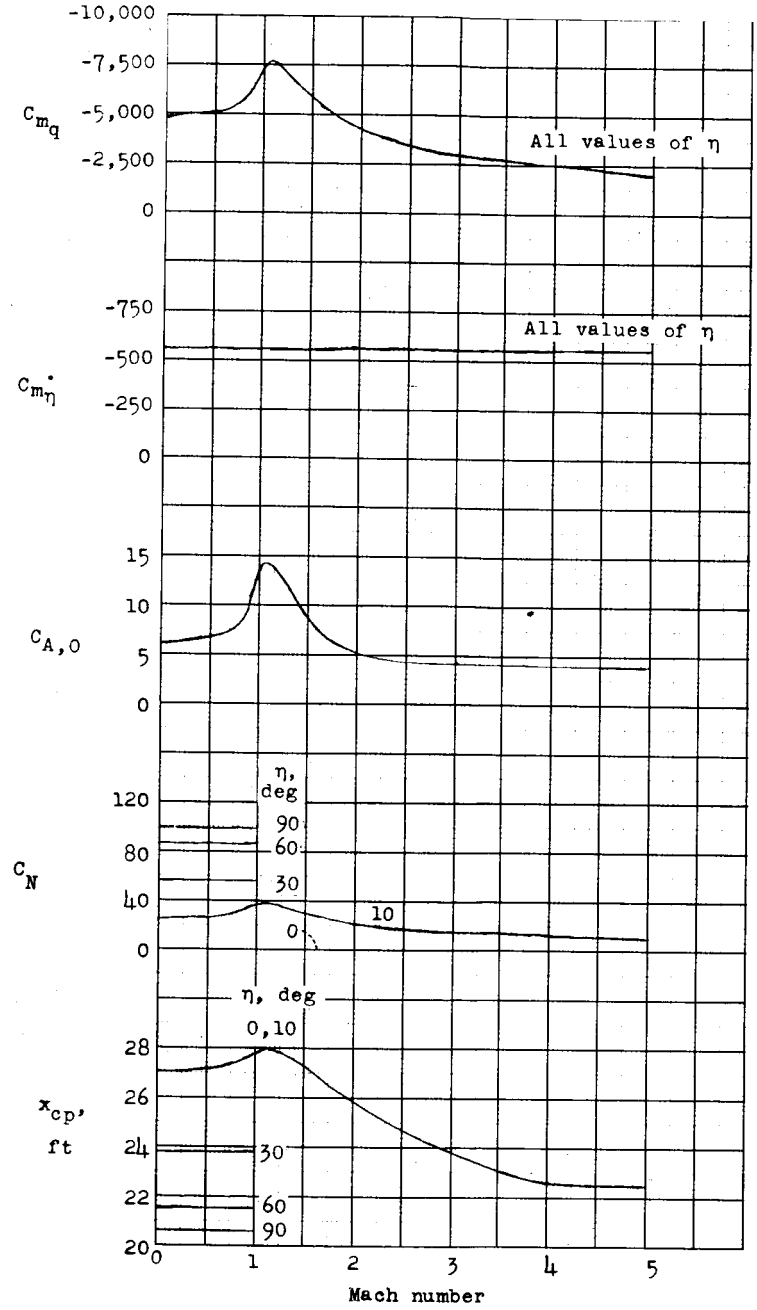


(a) Variation of $C_{m_q}$, $C_{m_{\dot{\eta}}}$, $C_{A,0}$, $C_N$, and $x_{cp}$ with Mach number.

Figure 2.- Shotput aerodynamic parameters.

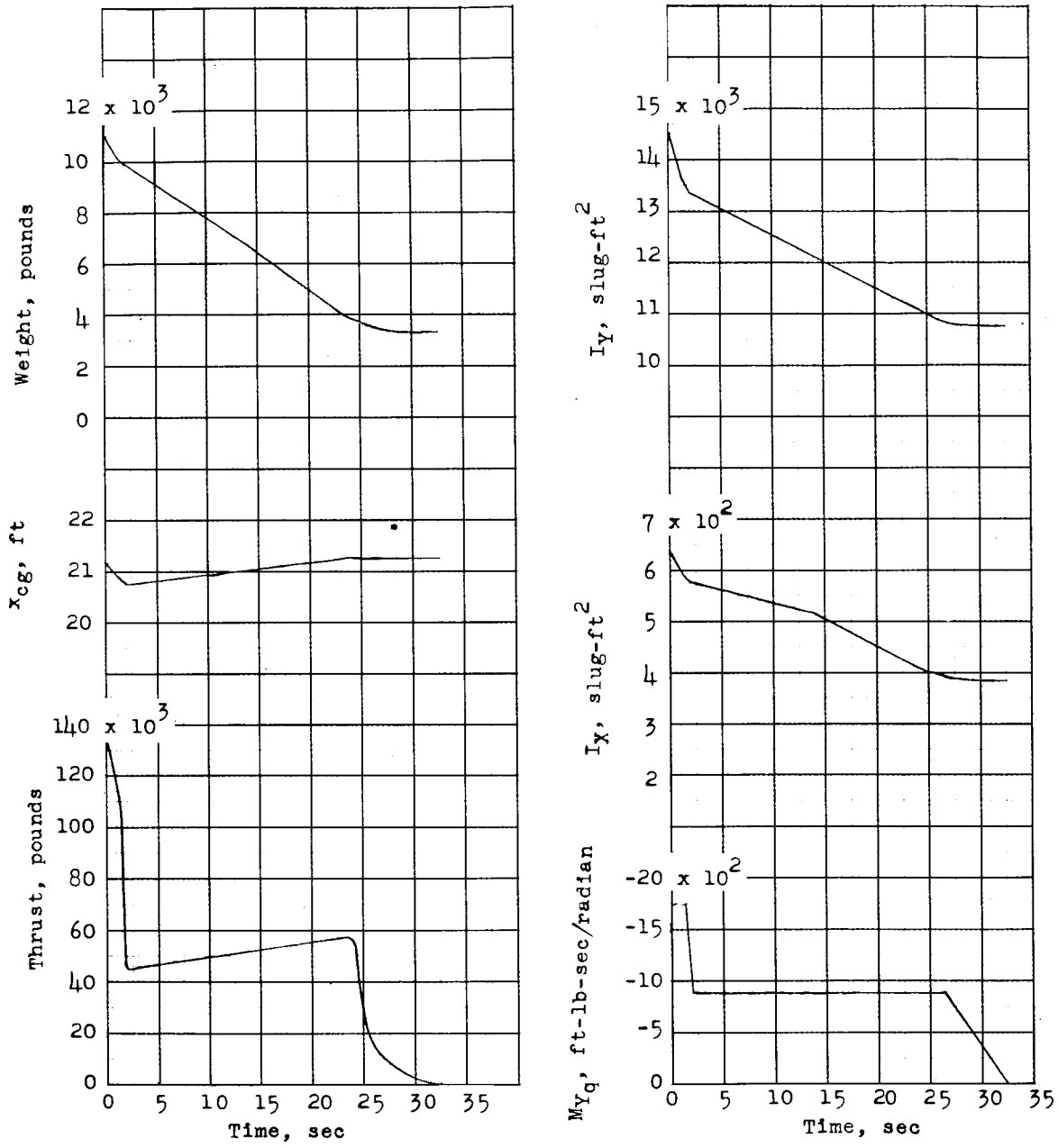


(b) Variation of weight, $x_{cg}$, thrust, $I_Y$, $I_X$, and $M_{Y_q}$ with time.

Figure 2.- Concluded.

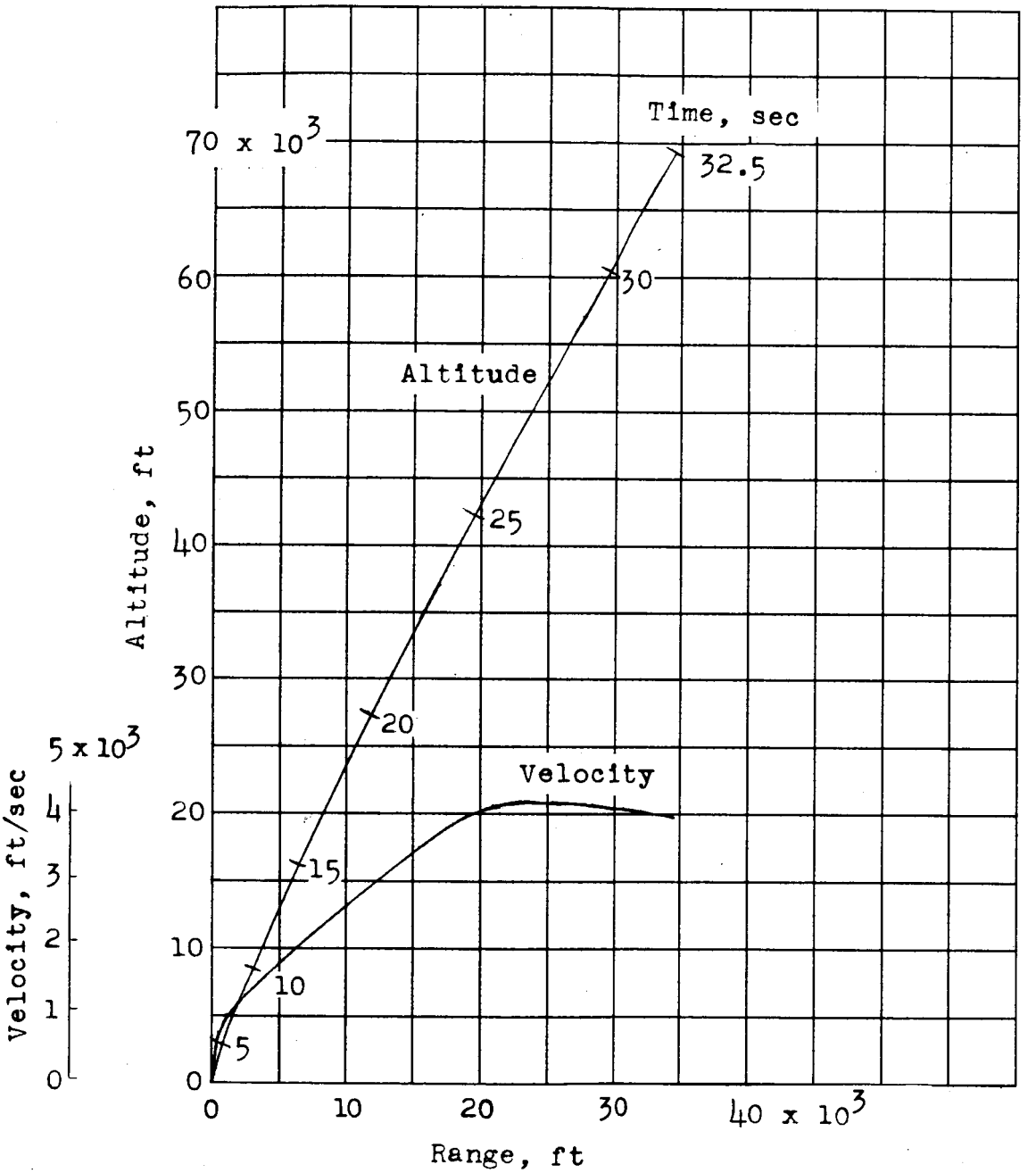


Figure 3.- Nominal Shotput performance during first-stage burning.

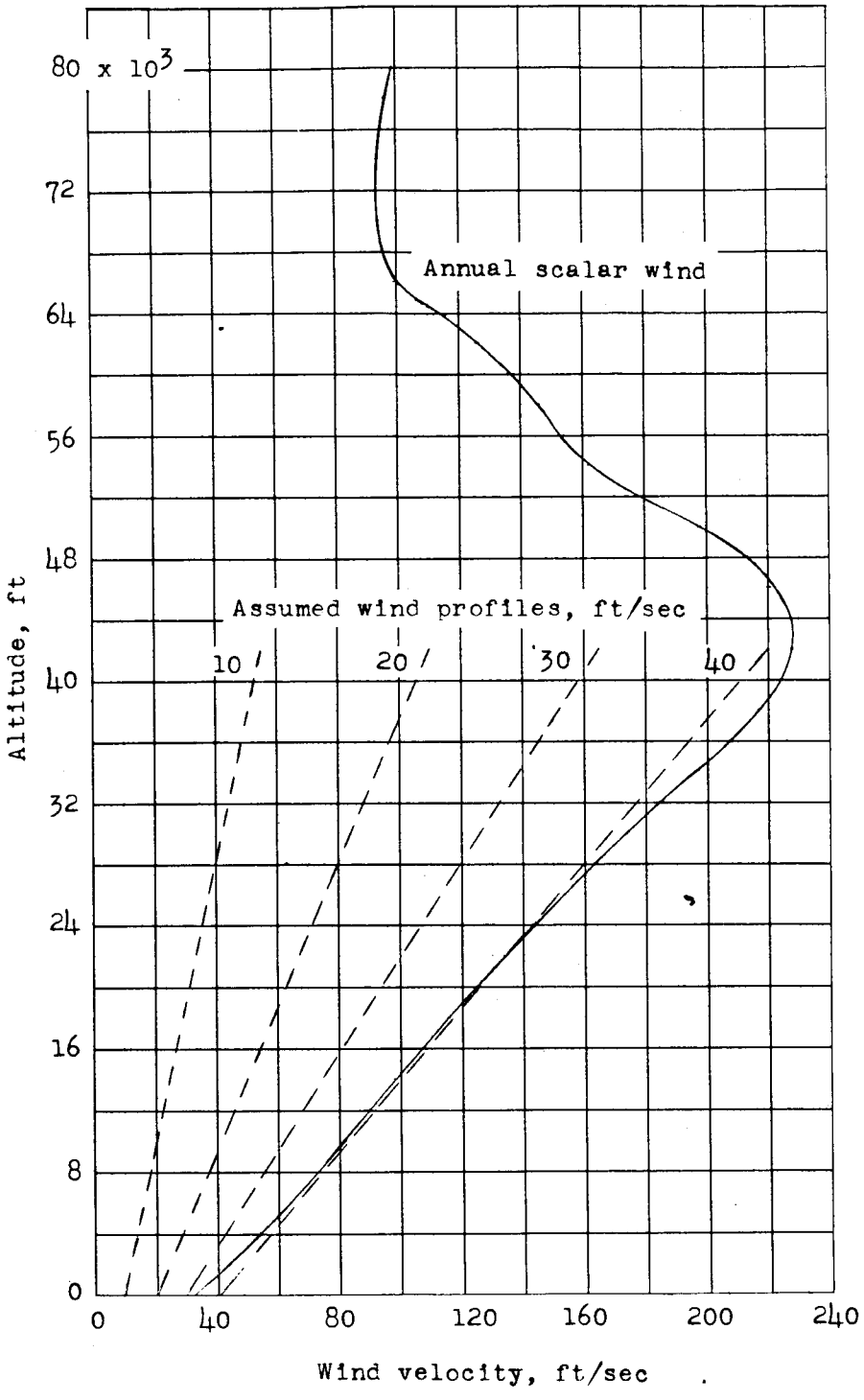


Figure 4.- Velocity profiles used in wind analysis.

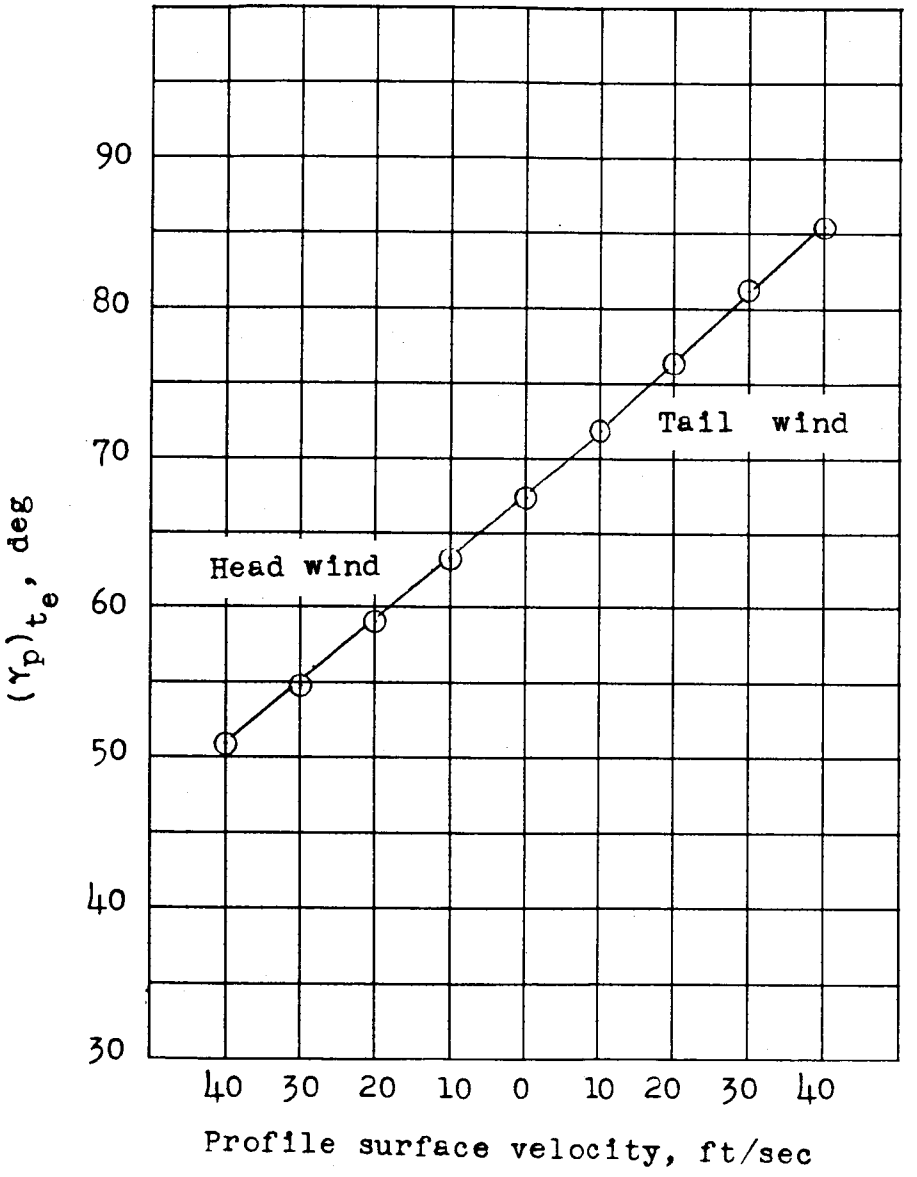


Figure 5.- Effect of head and tail winds on pitch flight-path angle at $t_e$ for the Shotput vehicle. $\gamma_{p,o} = 78^{\circ}$.

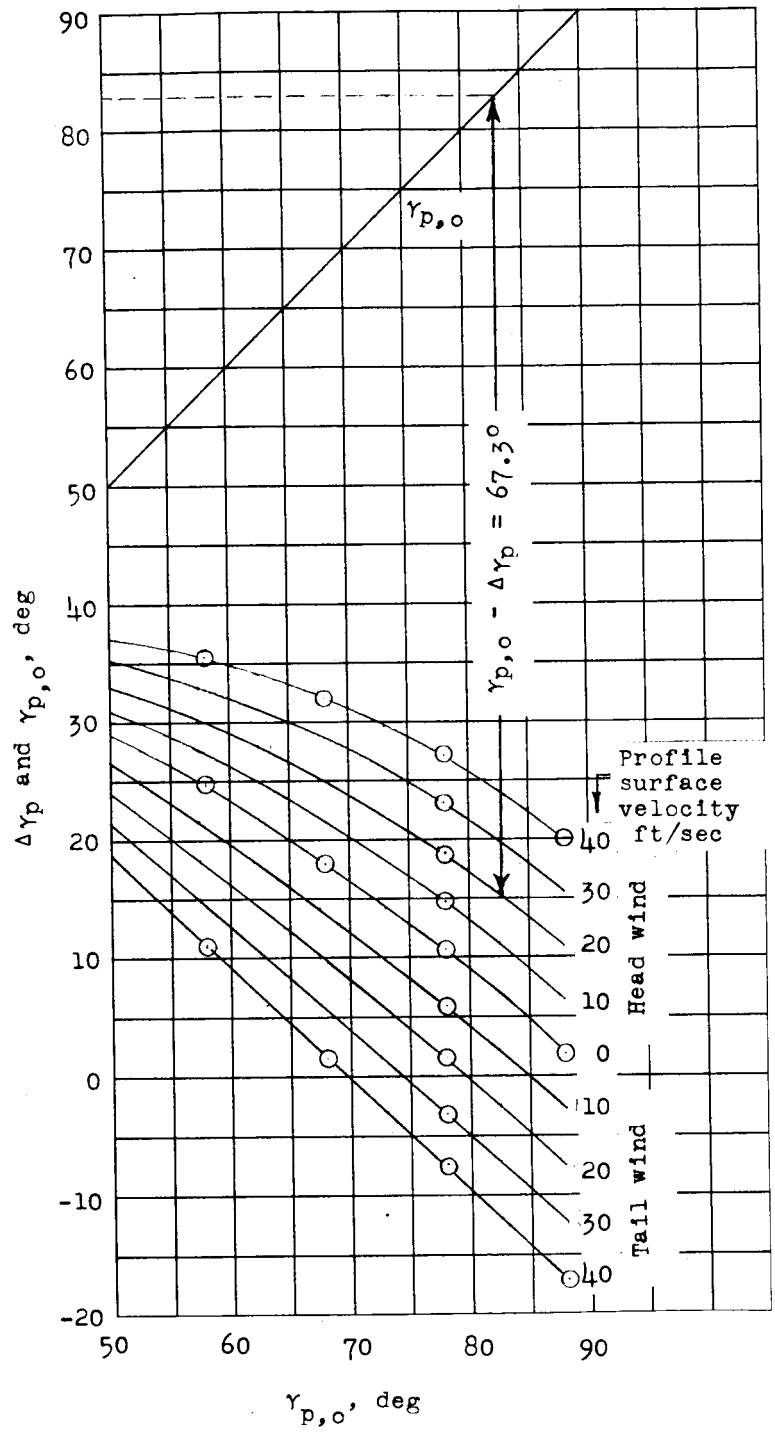


Figure 6.- Change in flight-path angle in pitch due to launch elevation for head and tail winds. Shotput vehicle.

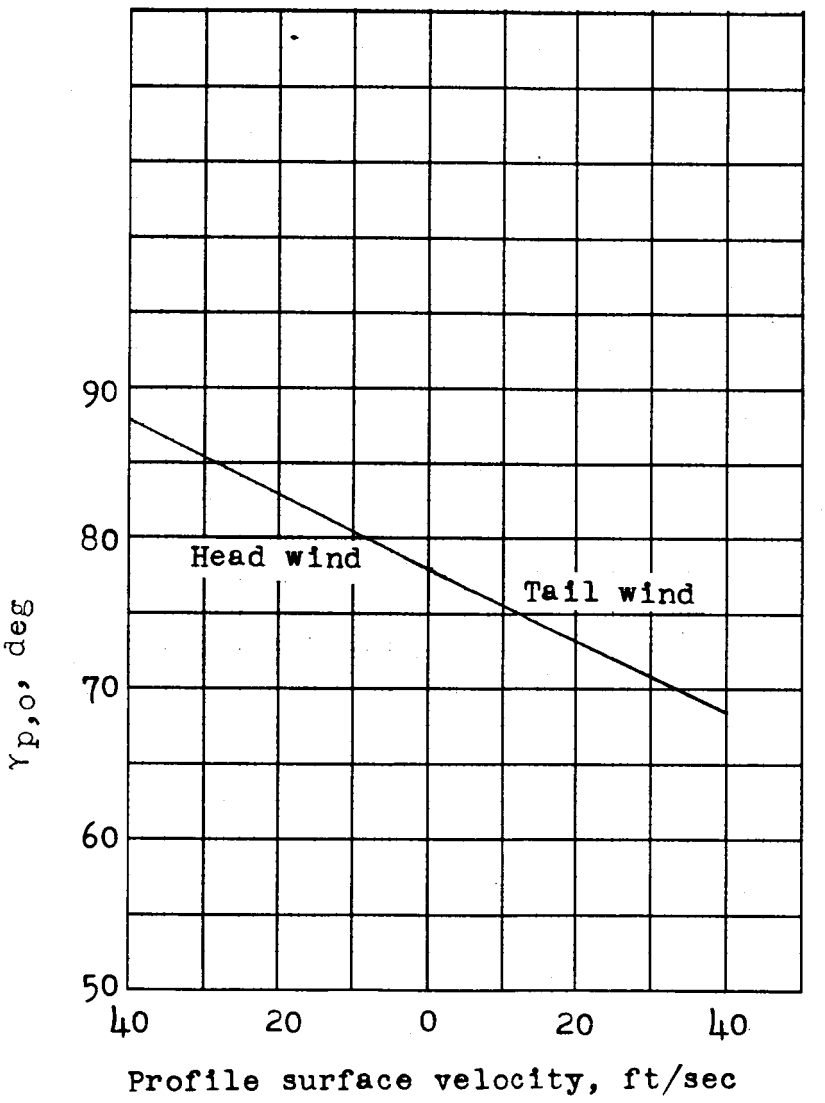


Figure 7.- Launch elevation for compensation of various head and tail winds. Shotput vehicle.

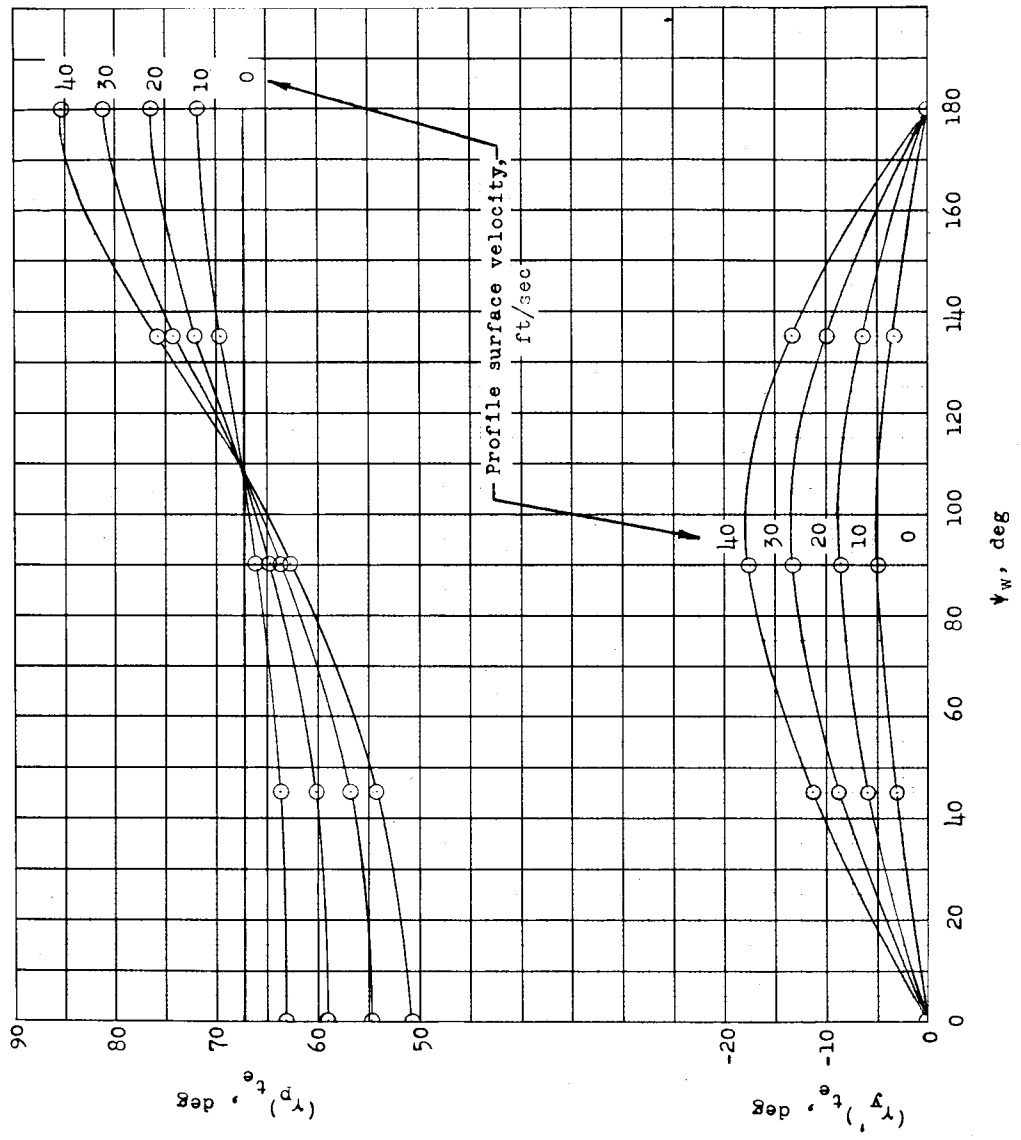


Figure 8.- Variation in flight-path angles in pitch and yaw at $t_e$ with wind velocity and angle for the Shotput vehicle. $\gamma_{p,o} = 78^\circ$.

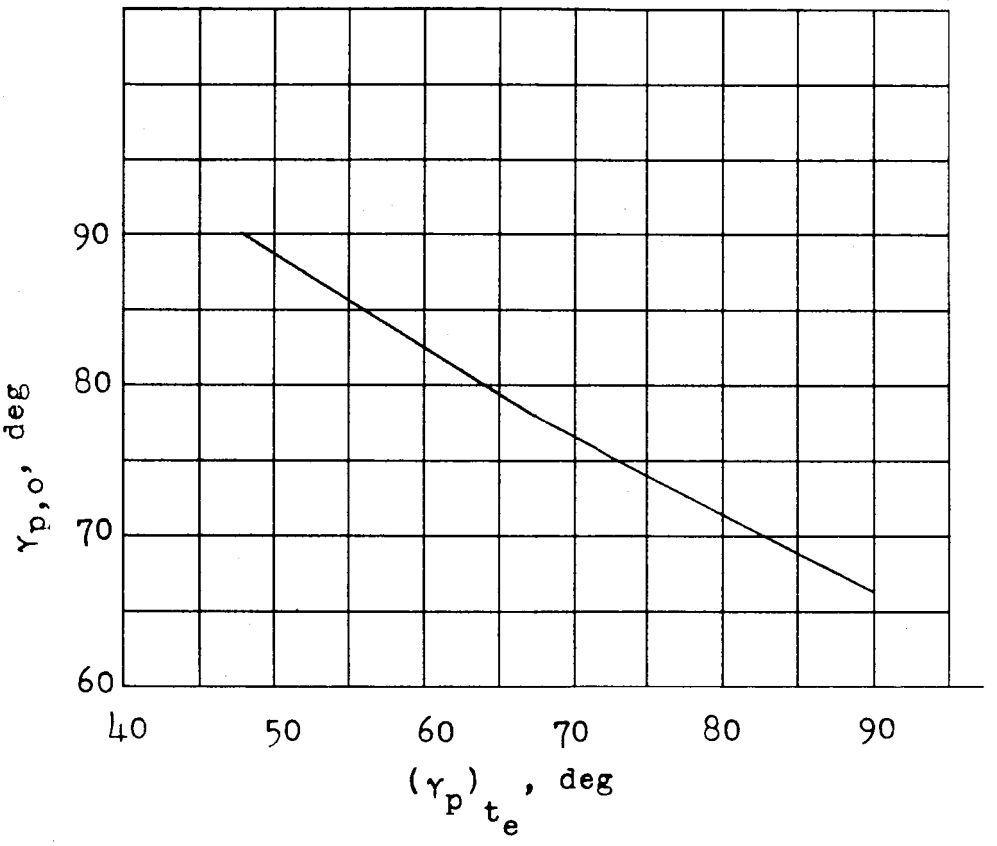


Figure 9.- Launch elevation for wind compensation as a function of $(\gamma_p)_{t_e}$ for the Shotput vehicle.

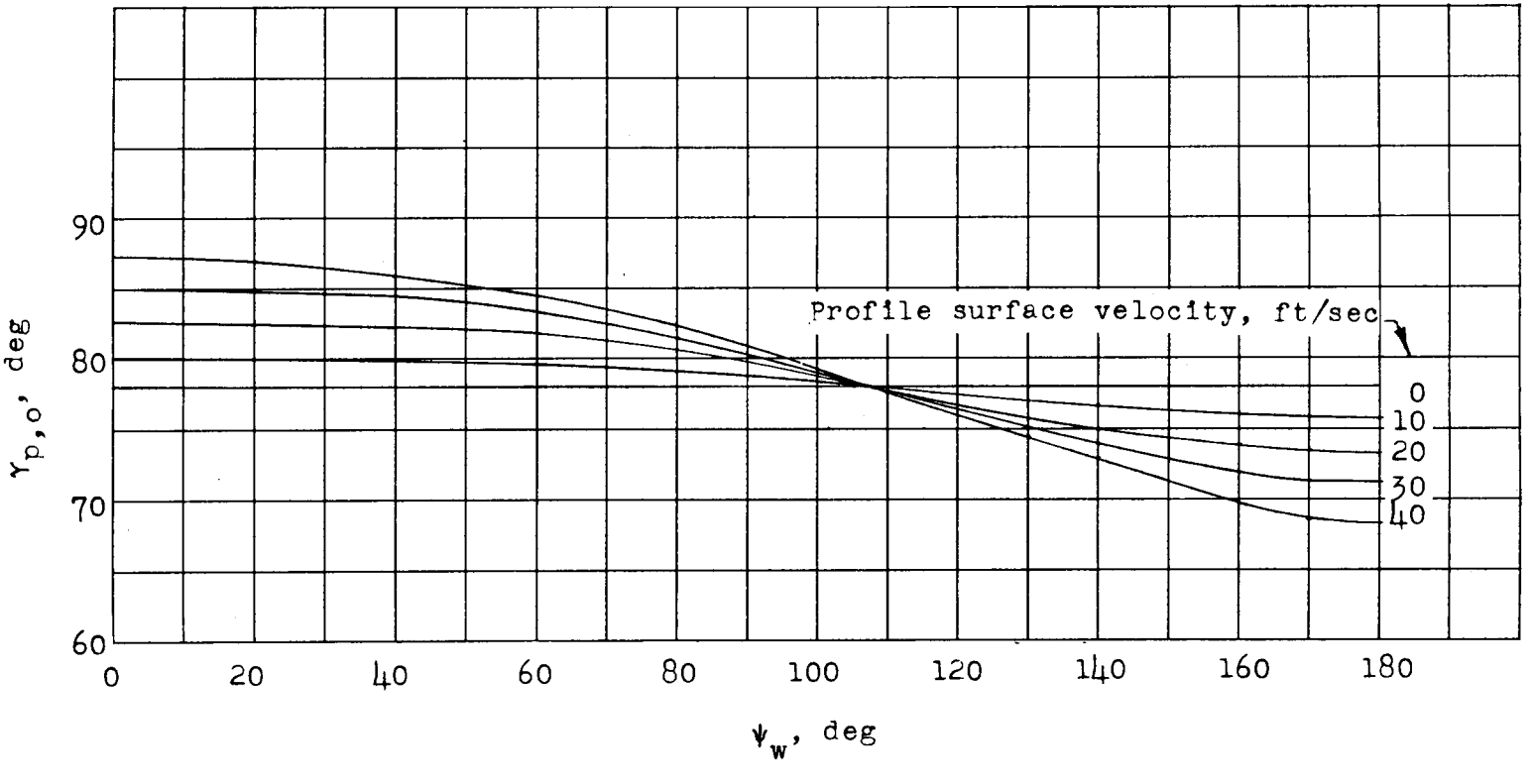


Figure 10.- Launch elevation for the Shotput vehicle to compensate for winds from various directions.

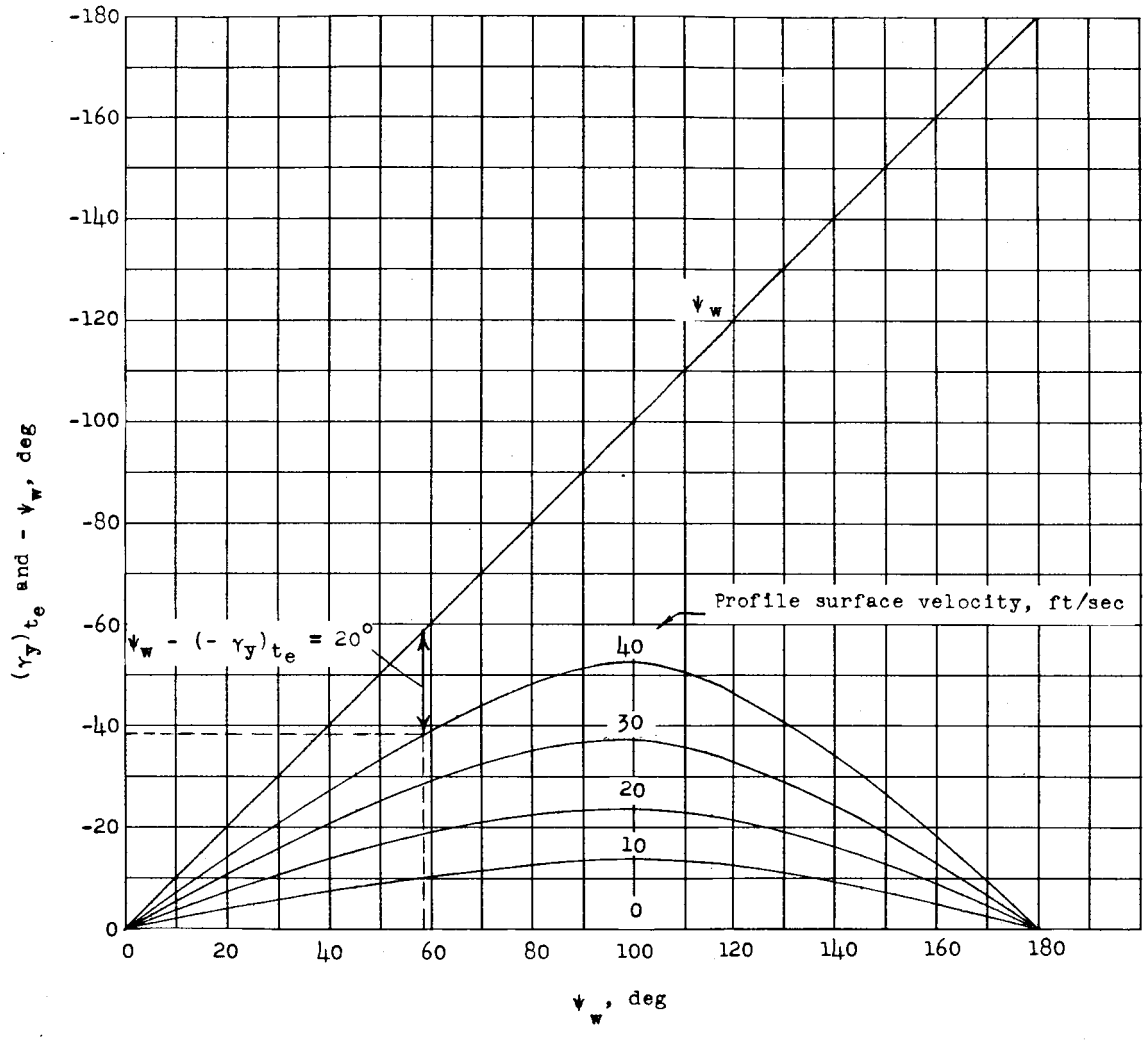


Figure 11.- Yaw angle in the earth plane due to winds from various directions. Shotput vehicle.

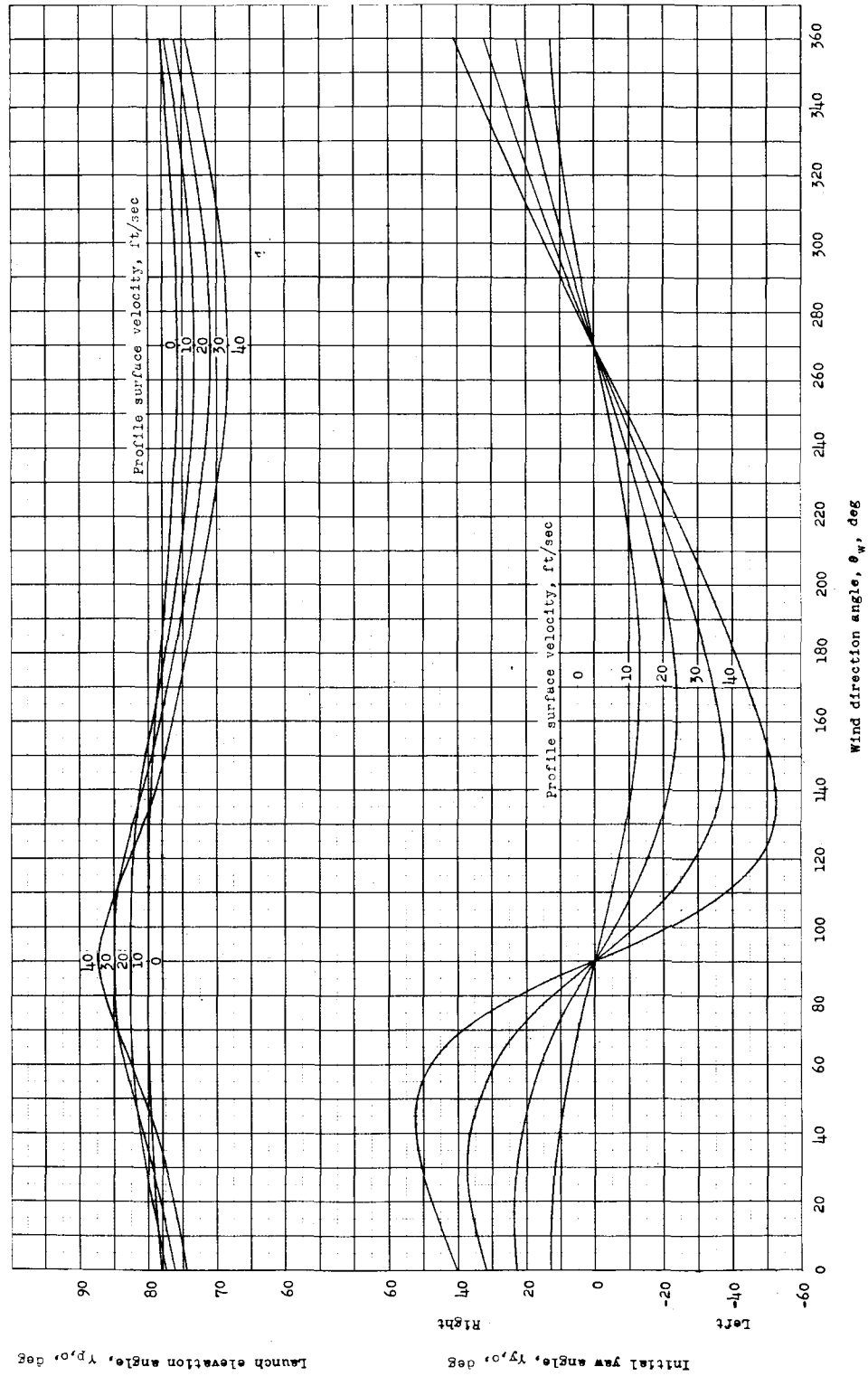


Figure 12.- Wind-compensation graph for Shotput vehicle.

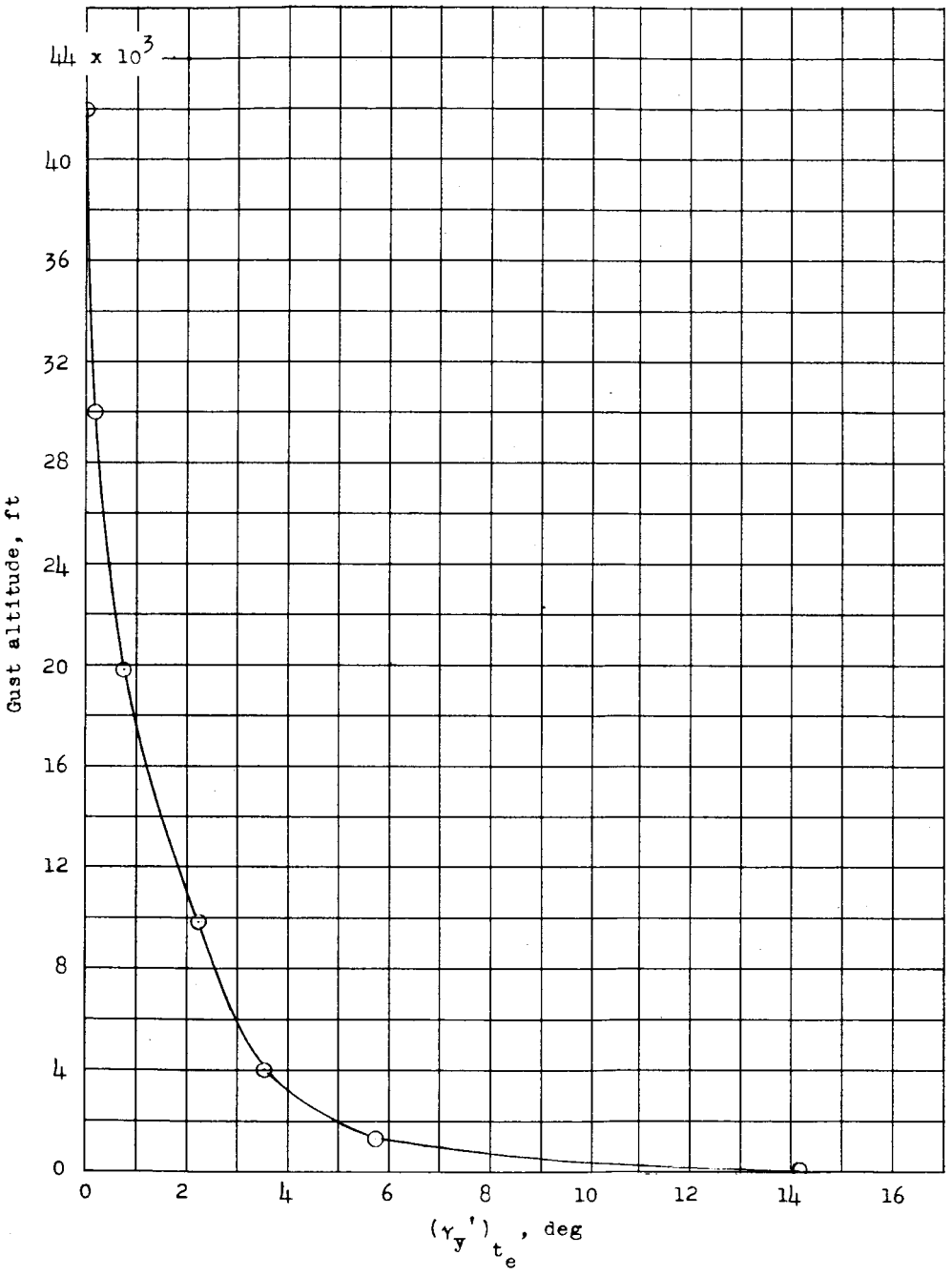


(a) Variation of $\left(\gamma_y'\right)_{t_e}$ with gust altitude.

Figure 13.- Shotput vehicle sensitivity variation with altitude.

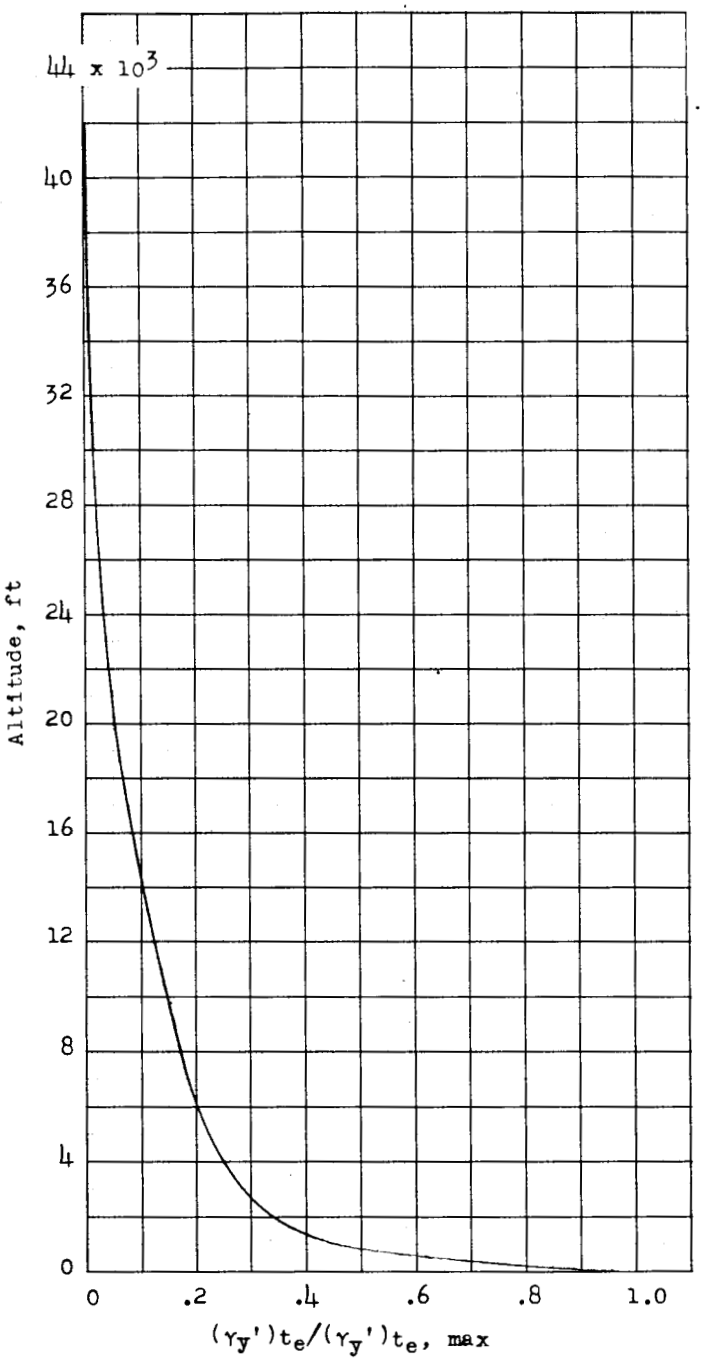


(b) Variation of $\gamma_y' \Big/ \left(\gamma_y'\right)_{max}$ with altitude.

Figure 13.- Concluded.

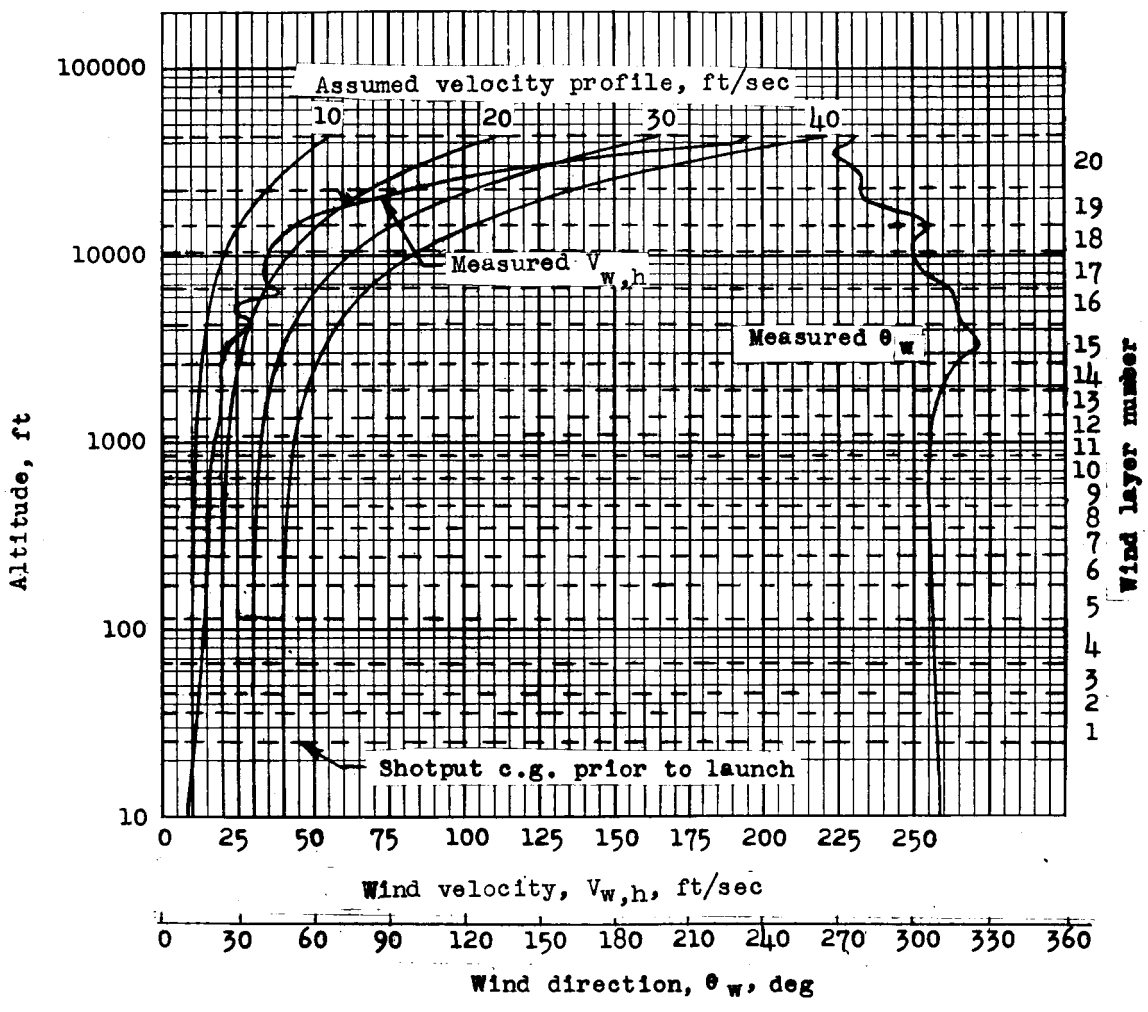


Figure 14.- Wind-weighting graph and wind data measured October 28, 1959, at NASA Wallops Station.

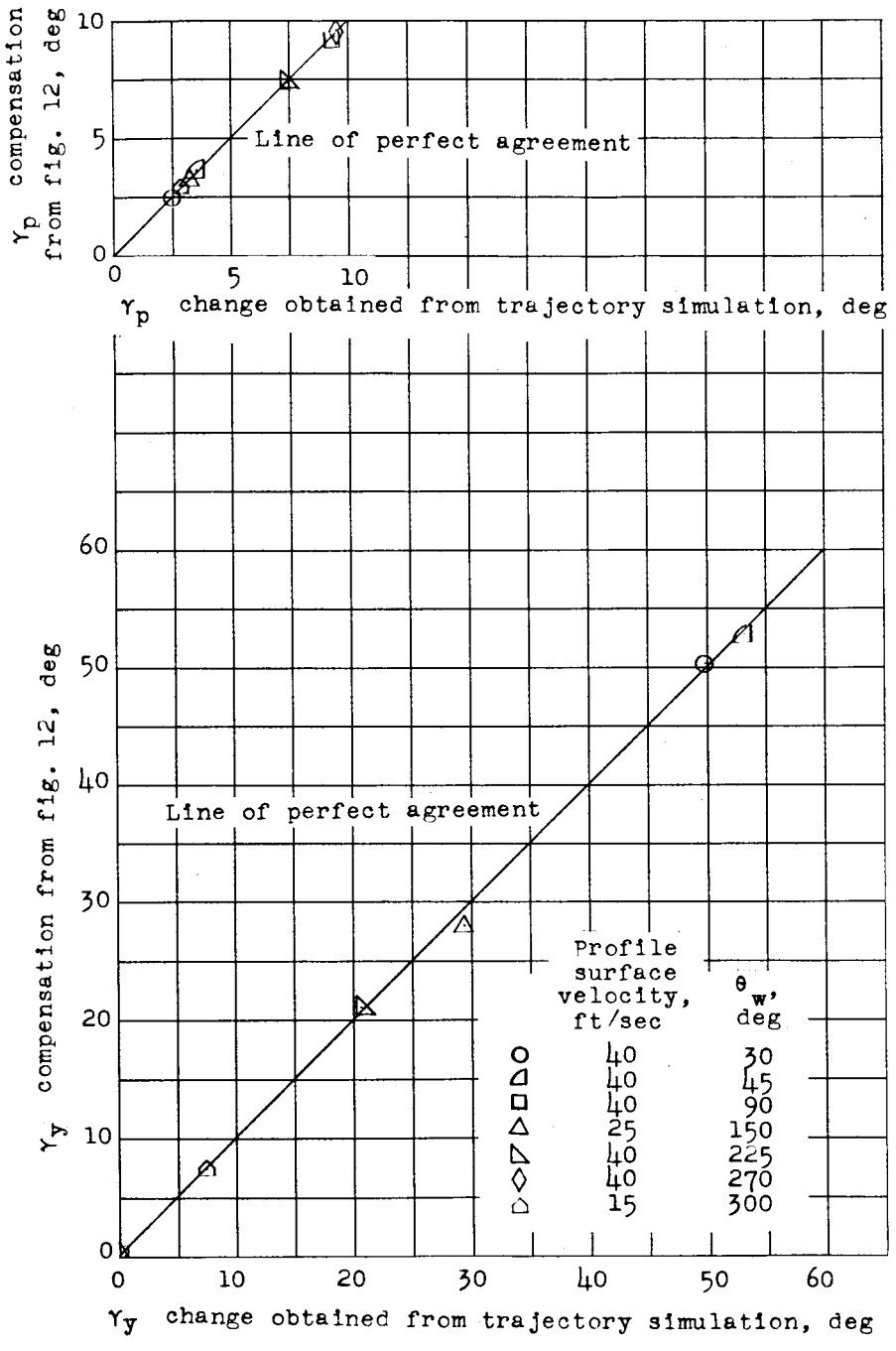


(a) Correlation between wind-compensation angles used and change obtained for assumed profiles.

Figure 15.- Wind analysis check.

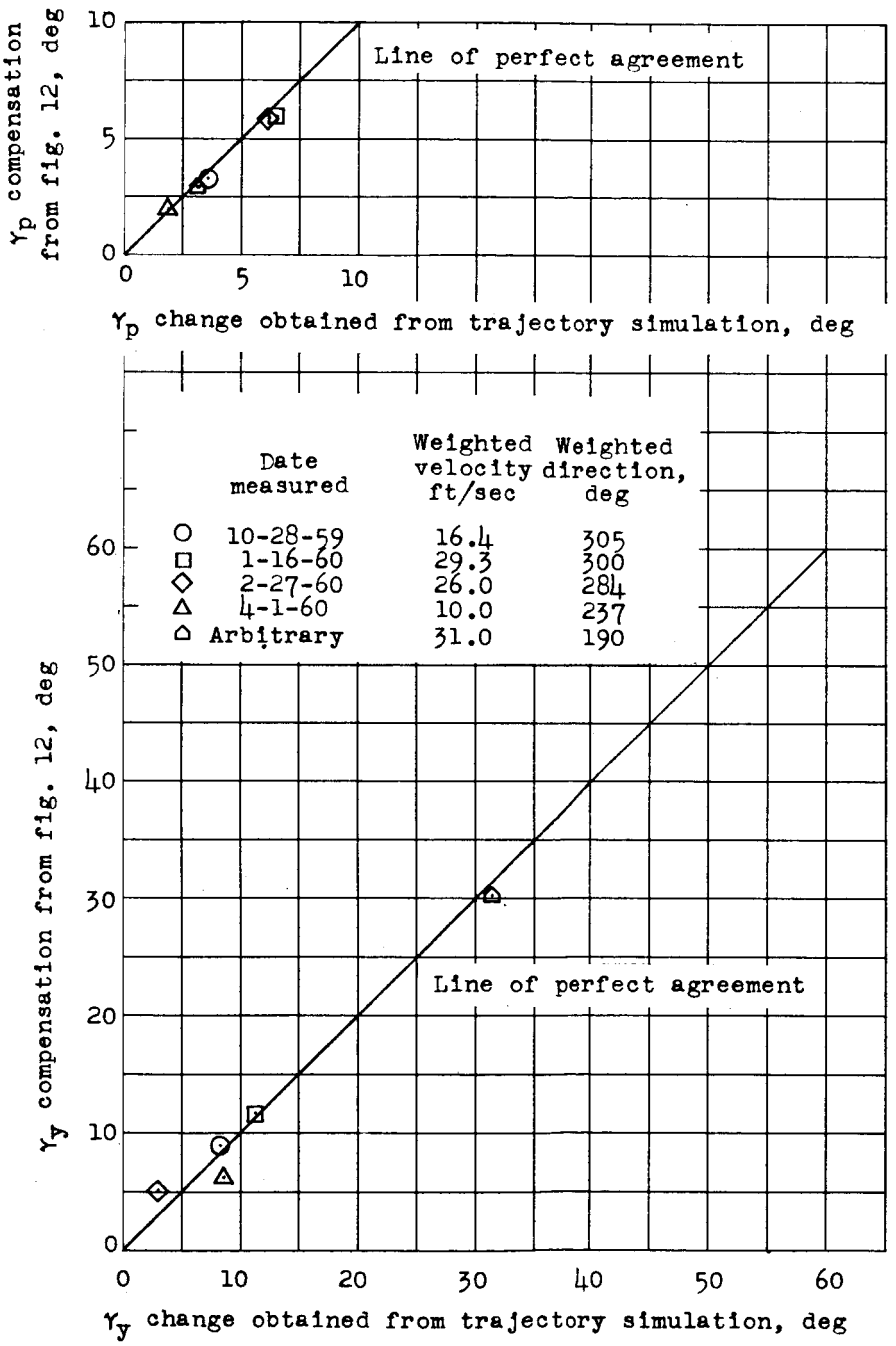


(b) Correlation between wind-compensation angles used and change obtained for measured winds.

Figure 15.- Concluded.

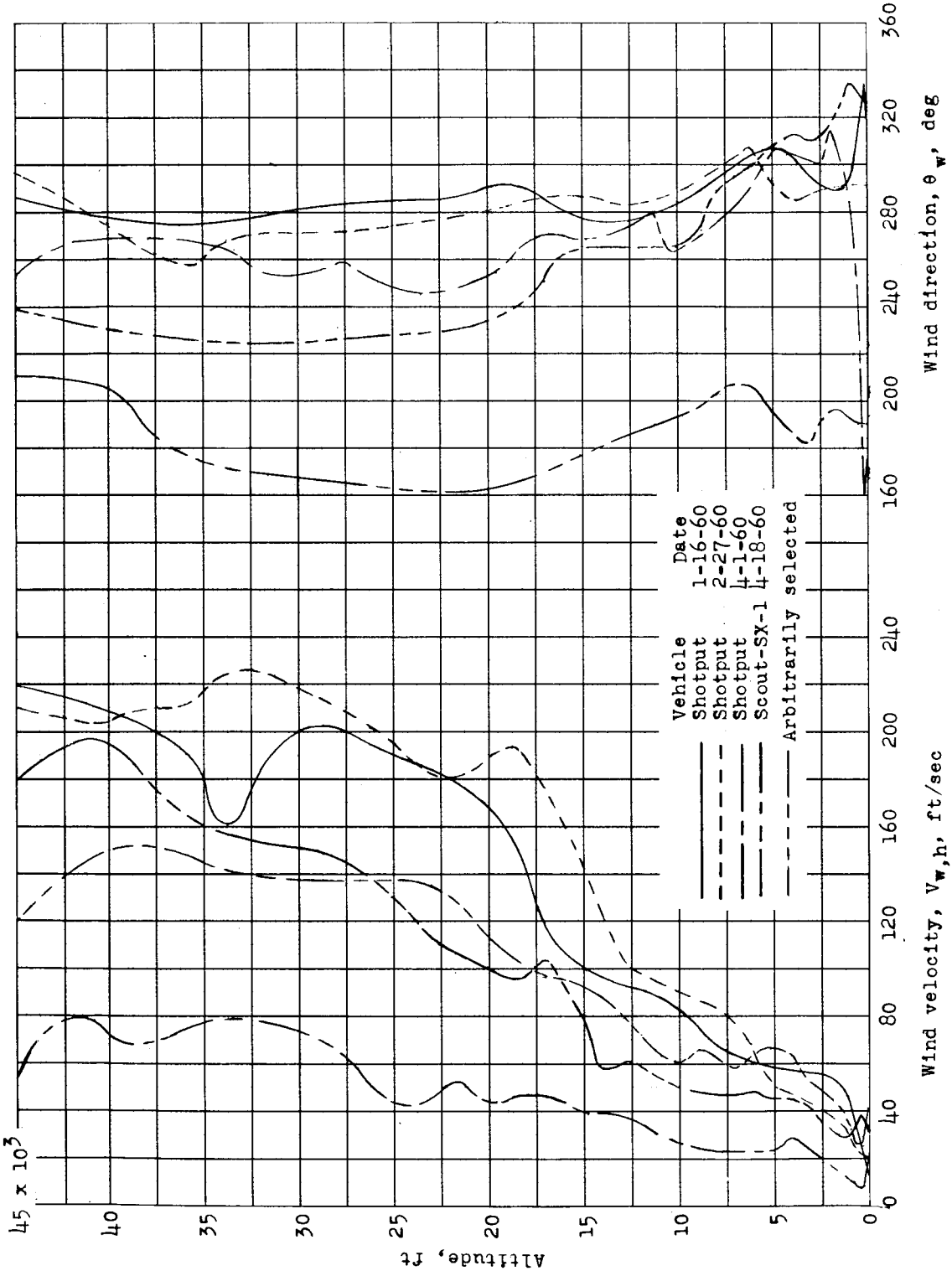


Figure 16.- Wind data.

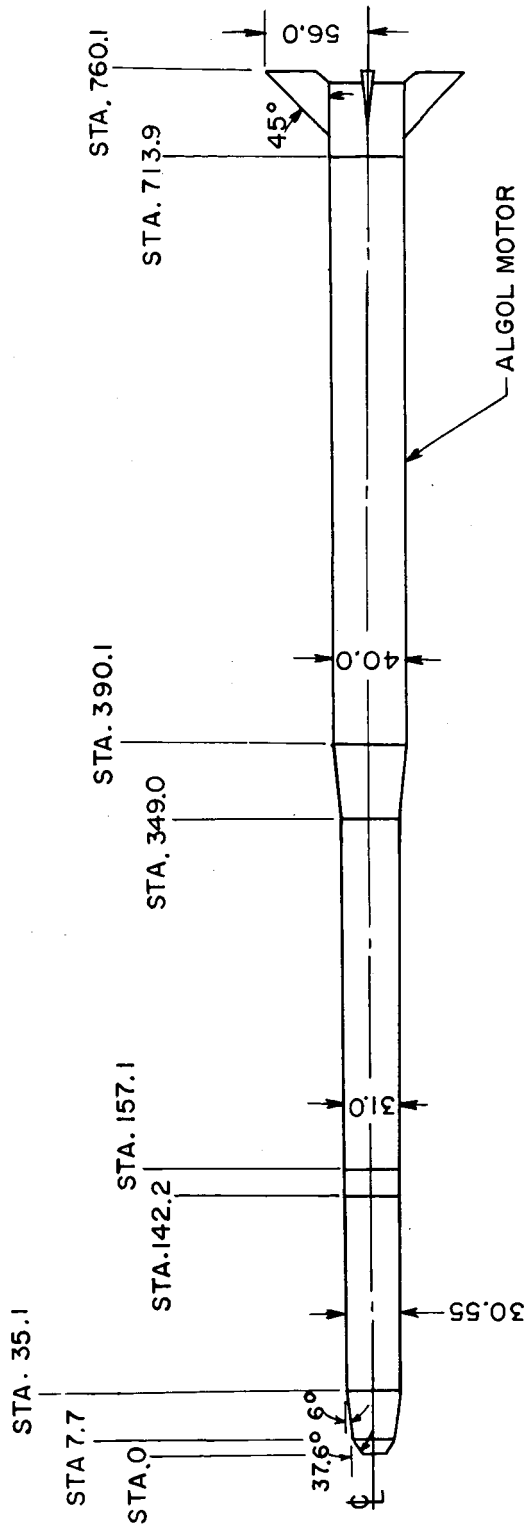


Figure 17.- General configuration of Scout-SX-1 vehicle.

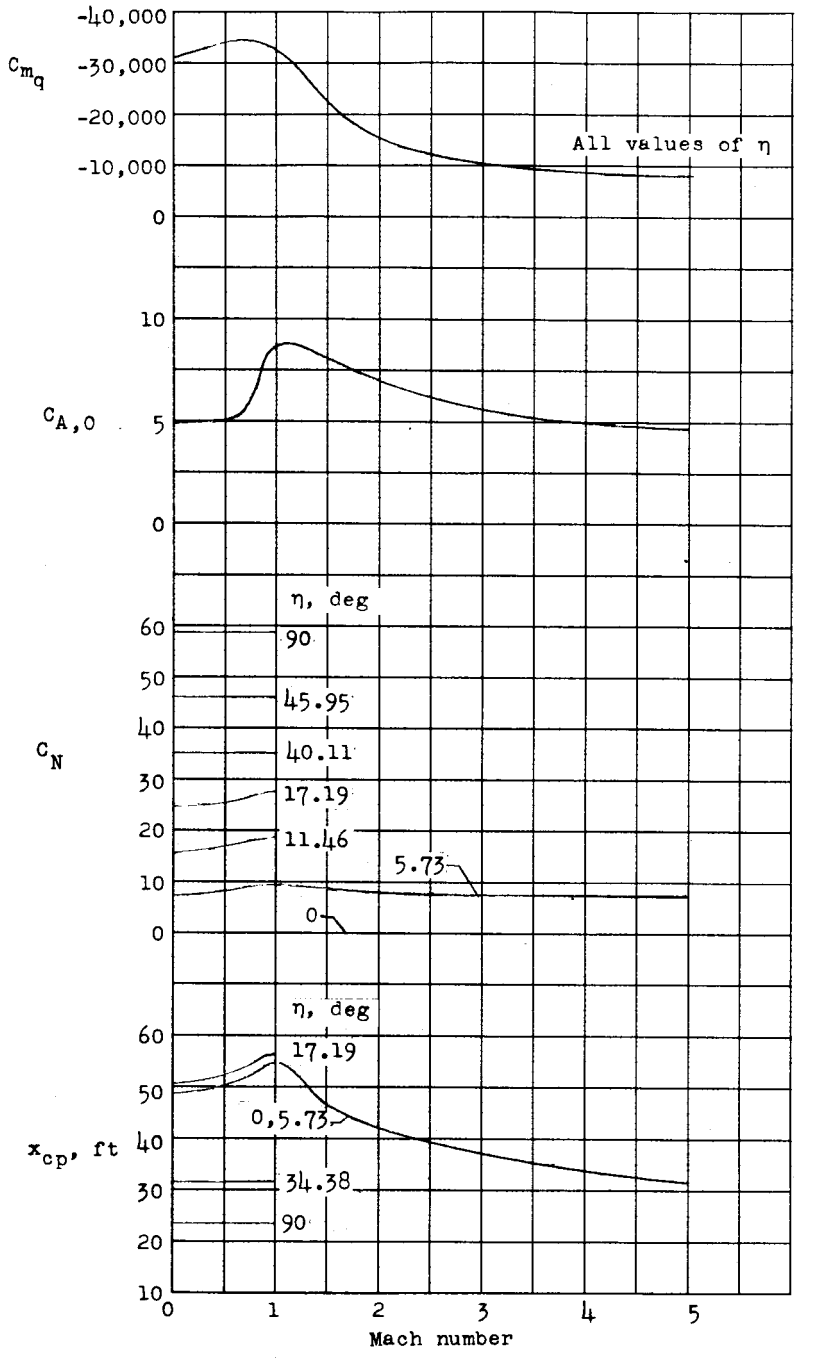


(a) Variation of $C_{m_q}$, $C_{A,0}$, $C_N$, and $x_{cp}$ with Mach number.

Figure 18.- Aerodynamic parameters for Scout-SX-1.

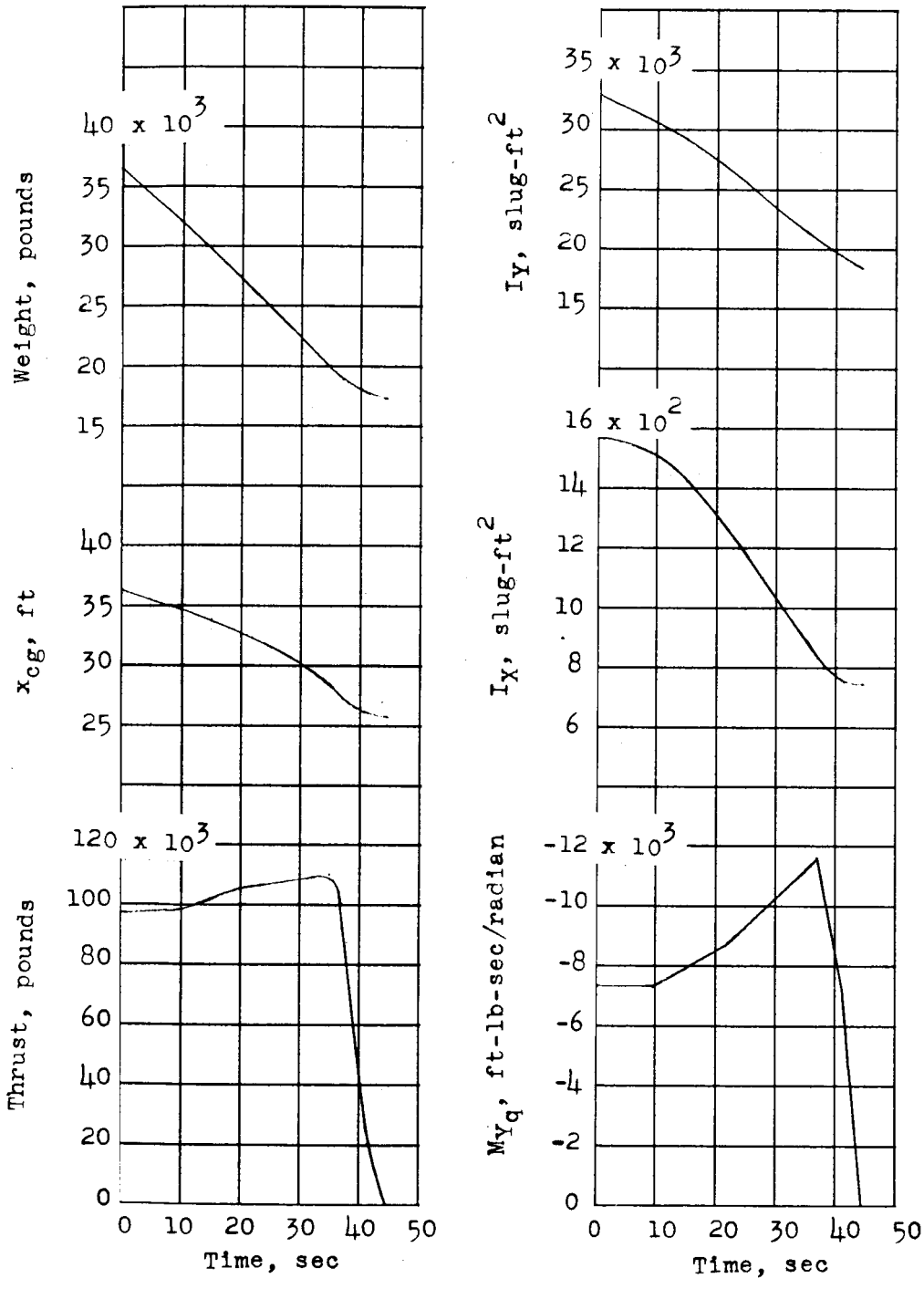


(b) Variation of weight, $x_{cg}$, thrust, $I_Y$, $I_X$, and $M_{Y_q}$ with time.

Figure 18.- Concluded.

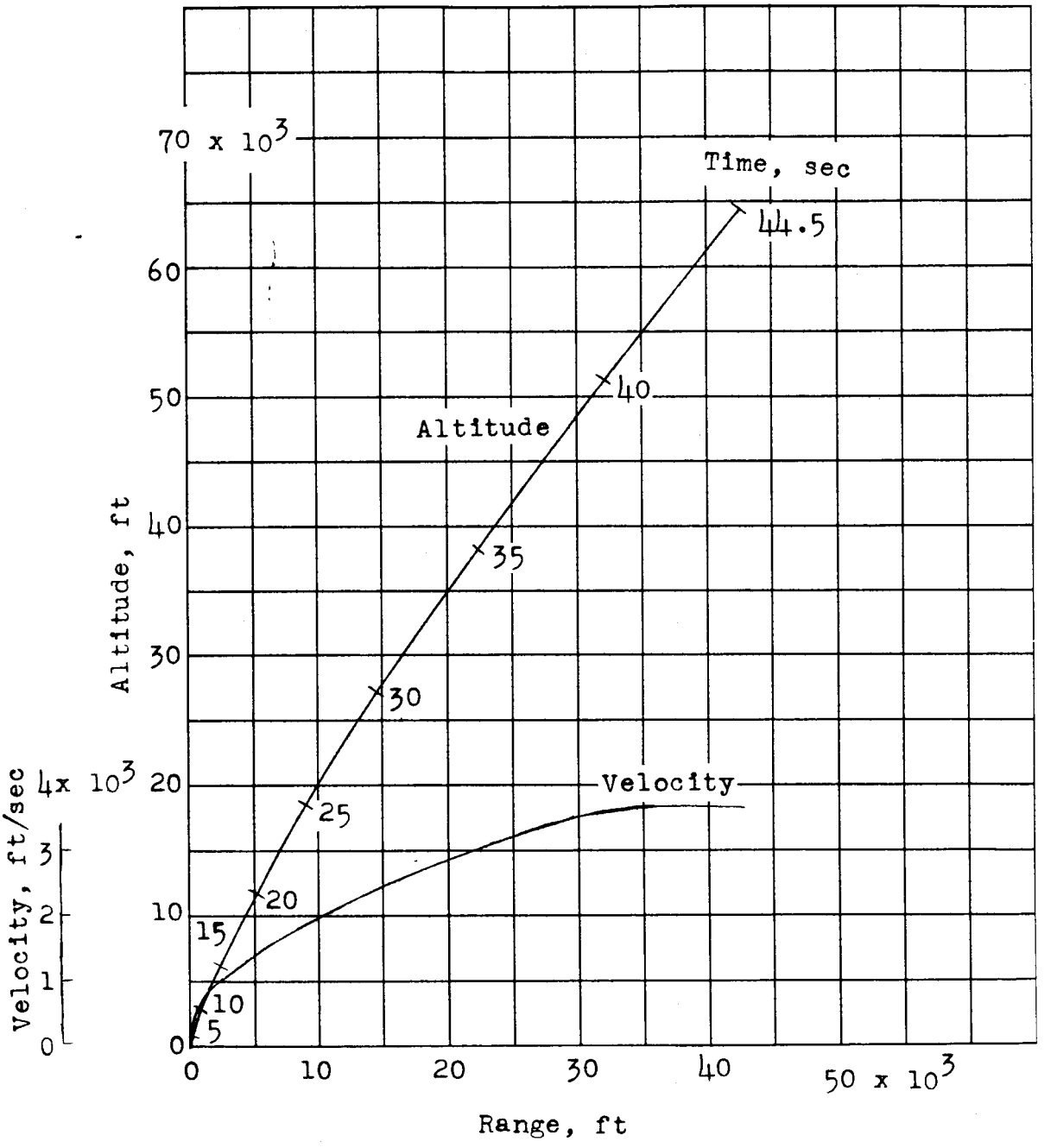


Figure 19.- Nominal Scout-SX-1 performance during first-stage burning.

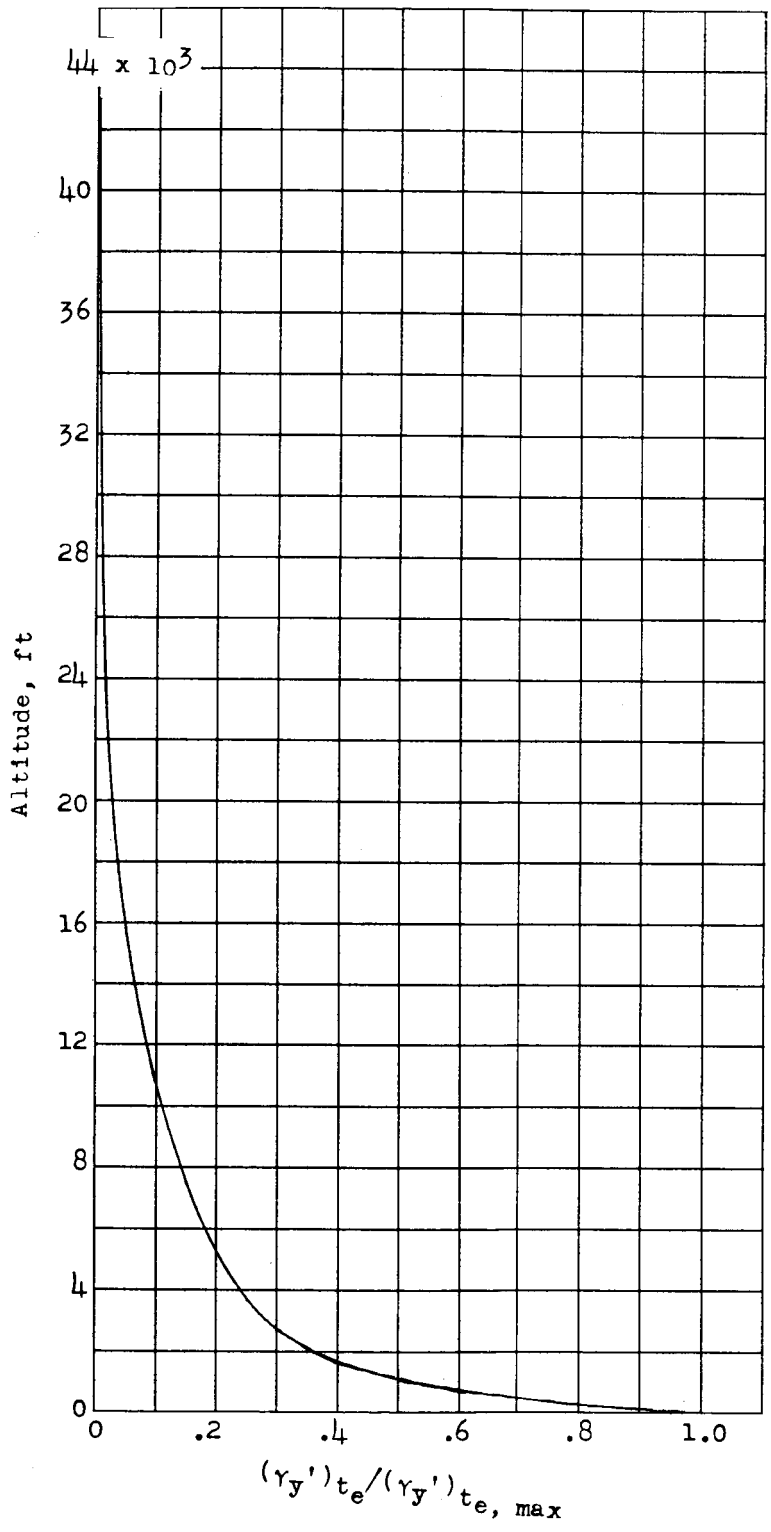


Figure 20.- Scout-SX-1 sensitivity variation with altitude.

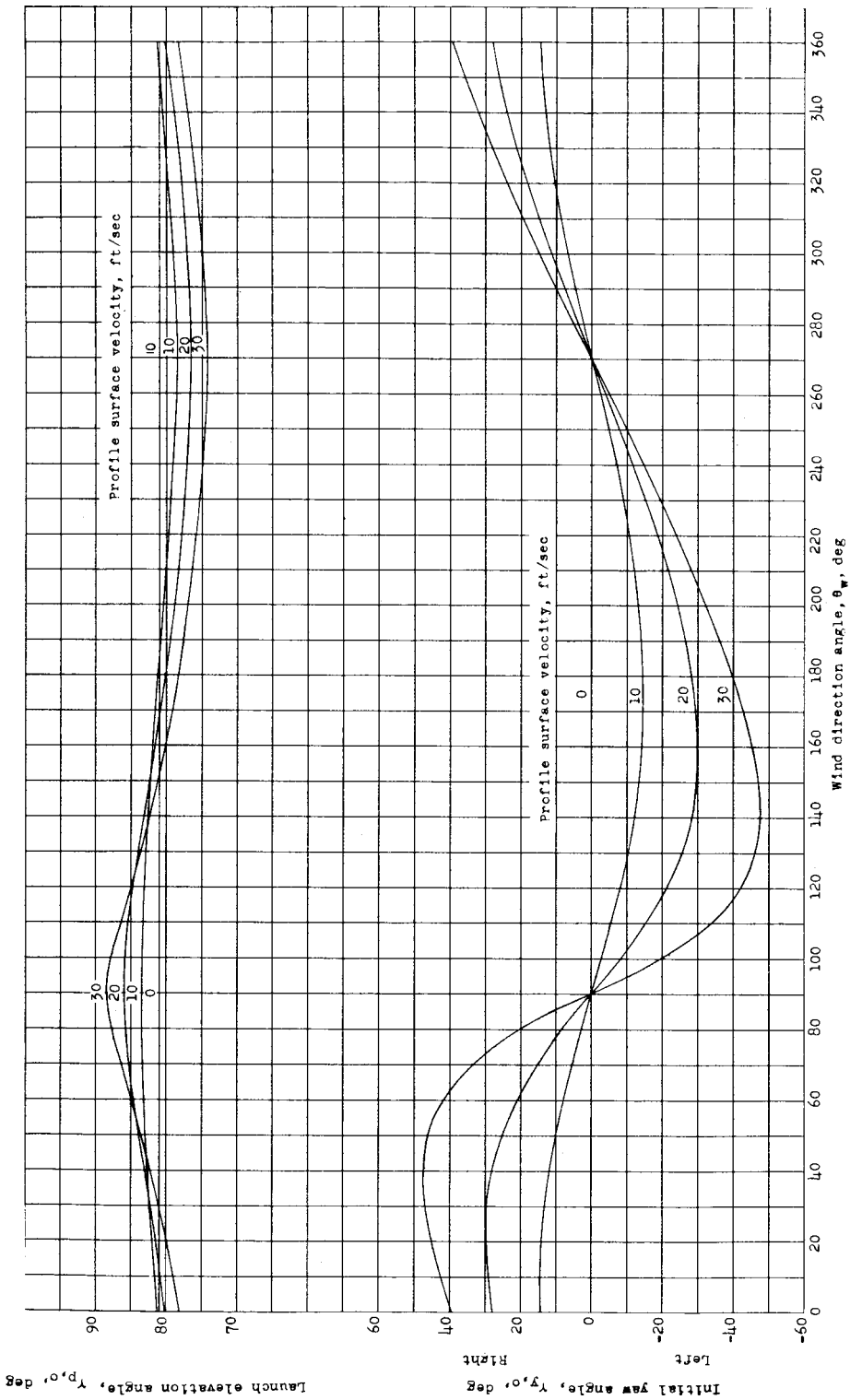


Figure 21.- Wind-compensation graph for Scout-SX-1 vehicle.